Heritability of hippocampal functional and microstructural organisation

Şeyma Bayrak (1, 2, 3)*, Reinder Vos de Wael (4)*, H. Lina Schaare (1, 2), Meike D. Hettwer (1, 2, 5, 6), Benoit Caldairou (7), Andrea Bernasconi (7), Neda Bernasconi (7), Boris C. Bernhardt (4)*, Sofie L. Valk (1, 2)*

(1) Otto Hahn Group Cognitive Neurogenetics, Max Planck Institute for Human Cognitive and Brain Sciences, Leipzig 04103, Germany
(2) Institute of Neuroscience and Medicine, Research Centre Jülich, Jülich 52428, Germany
(3) Department of Cognitive Neurology, University Hospital Leipzig and Faculty of Medicine, University of Leipzig, Leipzig 04103, Germany
(4) Multimodal Imaging and Connectome Analysis Laboratory, McConnell Brain Imaging Centre, Montreal Neurological Institute, McGill University, Montreal, QC H3A 2B4, Canada
(5) Institute of Systems Neuroscience, Medical Faculty, Heinrich Heine University Düsseldorf, Düsseldorf, Germany
(6) Max Planck School of Cognition, Max Planck Institute of Human Cognitive and Brain Sciences, Leipzig 04103, Germany
(7) Neuroimaging of Epilepsy Laboratory, McConnell Brain Imaging Centre, Montreal Neurological Institute, McGill University, Montreal, QC H3A 2B4, Canada

Correspondence to Şeyma Bayrak and Dr. Sofie L. Valk
Email: bayrak@cbs.mpg.de, valk@cbs.mpg.de

Keywords: hippocampus, hippocampal subfields, gradients, heritability, microstructure, functional connectivity

* *These authors contributed equally.*

Highlights

1. Hippocampal organizational features are linked across structures and modalities.
2. Functional connectivity between hippocampal subfields and isocortex is heritable.
3. Microstructural variation along hippocampal subfields is highly heritable.
4. We find systematic genetic correlation with microstructure of the isocortex.
5. Genetic factors organize the hippocampal formation at the individual level.

Abstract

The hippocampus is a uniquely infolded allocortical structure in the medial temporal lobe that consists of the microstructurally and functionally distinct subregions: subiculum, cornu ammonis, and dentate gyrus. The hippocampus is a remarkably plastic region that is implicated in learning and memory. At the same time it has been shown that hippocampal subregion volumes are heritable, and that genetic expression varies along a posterior to anterior axis. Here, we studied how a heritable, stable, hippocampal organisation may support its flexible function in healthy adults. Leveraging the twin set-up of the Human Connectome Project with multimodal neuroimaging, we observed that the functional connectivity between hippocampus and cortex was heritable and that microstructure of the hippocampus genetically correlated with cortical microstructure. Moreover, both functional and microstructural organisation could be consistently captured by anterior-to-posterior and medial-to-lateral axes across individuals. However, heritability of functional, relative to microstructural, organisation was found reduced, suggesting individual variation in functional organisation may be explained by experience-driven factors. Last, we demonstrate that structure and function couple along an inherited macroscale organisation, suggesting an interplay of stability and plasticity within the hippocampus. Our study provides new insights on the heritability of the hippocampal of the structure and function within the hippocampal organisation.

Introduction

The hippocampal formation in the medial temporal lobe is involved in numerous functions such as episodic memory [1–3], spatial navigation [4], emotional reactivity [5] and stress resilience [6–8]. It is a region highly susceptible to disorder in various neurological and neuropsychiatric conditions, such as schizophrenia [9], posttraumatic stress disorder [10], temporal lobe epilepsy [11], and Alzheimer's disease [12]. Having a three layered allocortex, the hippocampal formation consists of multiple subfields, or zones, starting at the subiculum (SUB) and moving inward to the hippocampus proper; the cornu ammonis (CA), and dentate gyrus (DG) [13–16]. These subfields have unique microstructure [15,16] and participate differently in the hippocampal circuitry [17], likely implicating different contributions to function [18–20]. Beyond the internal hippocampal wiring, anatomical projections to isocortical targets vary based on the position within the hippocampal formation [21,22]. Thus, the intrinsic organisation of the hippocampus relates to its connectivity to the rest of the brain. For example, tracer studies in rodents have shown that the ventral hippocampus is anatomically connected to the olfactory regions, prefrontal cortex, and amygdala, while the dorsal hippocampus is connected to the retrosplenial cortex, mammillary bodies, and anterior thalamus [23,24]. This ventral-dorsal transition in rodents may relate to an anterior-posterior (A-P) axis in humans [25,26]. Conversely, hippocampal infolding aligns with a medial-lateral (M-L) axis followed by the subfields, suggesting another transitional axis driven by intracortical microstructure [16,27]. Thus, the hippocampal formation features two major axes, one from anterior to posterior segments, and the other along its infolding from SUB via CA to DG.

Hippocampal organisational axes can be described using gradients [28]. This framework enables continuous representations of the high-dimensional inter-regional patterns, unrestricted by the traditional network boundaries [29 30]. Along each gradient axis, voxels/vertices sharing similar connectivity patterns are situated close to each other, whereas those most divergent are at opposite ends of the respective axis [31]. Using this method, hippocampal organisational axes observed in the structure of the hippocampus have been reported to be paralleled by the functional organisation of the hippocampus, as measured *in vivo* using functional MRI [32 33–35]. Hippocampal gradients were further associated with its microstructural organisation [35], as well as performance on memory recollection [34] and pattern separation tasks [33], suggesting a link between functional organisation of the hippocampus, its structure, and behavioural variability. At the same time, whether hippocampal

functional and microstructural organisation axes vary according to genetic factors or rather adapt flexibly as a function of environment is incompletely understood.

There is ample evidence that individual variation on the organization of the hippocampal formation is shaped by both genetic and environmental factors. Indeed, various studies in non-human mammals have indicated unique plasticity of the hippocampal formation associated with its different subfields and underlying microstructural variations [36,37]. Though studies on genetic and environmental impact on individual variation of hippocampal structure and function in humans are limited relative to work in animal models, various studies have reported subfield heritability [38–40]. Moreover, genome-wide studies identified single-nucleotide polymorphisms (SNP) associated with hippocampal volumes [41–44] showing, in part, unique SNPs for each subfield and furthermore associated with neuropathology of schizophrenia [45,46]. Importantly, heritability provides an estimate to what extent genetic and environmental factors may impact a given trait as it provides a, sample specific, upper limit on the amount of variance explained by genetic factors. This is particularly relevant given that the individual variation in hippocampus is likely also partly explained by non-genetic factors. For example, the unique plasticity of hippocampal formation is associated with its different subfields and, amongst others, affected by the hormonal levels and stress responses [47,48]. Such environmentally-induced plasticity has also been shown in humans, such as variation in hippocampal structure due to variation hormonal status [49,50] and stress levels [51]. A second way to reconcile the notion of plasticity and stability reported in the hippocampus is by means of the structural model [52]. This model links isocortical cytoarchitecture and associated connectivity patterns to regional variations in plasticity and stability [53–56]. In the isocortex, structure-function coupling has been shown to progressively decrease along an axis from unimodal to transmodal regions [57–60]. Such uncoupling is paralleled by reductions in genetic control from unimodal to transmodal regions [61]. It is possible that the coupling of microstructure and function in the hippocampus shows meaningful variation along its large-scale axes, and helps to further understand the interrelation between plasticity and stability, or genetic and environmental factors, within this allocortical structure."

Here, we studied to what extent hippocampal function and structure is heritable and shows a genetic correlation with the cortex. To do so, we leveraged the multimodal dataset of the Human

Connectome Project [62] to sample resting state functional time series as well as T1w/T2w intensity (as a proxy for intracortical myelination [63]) in both the hippocampal subfields and isocortex. Our method of choice was the connectivity gradients approach across all hippocampal subfields rather than network parcellation approaches. Connectivity gradients situate brain areas in a continuous fashion based on their functional connectome patterns, whereas the network parcellations draw sharp boundaries [64]. Indeed, recent work has indicated that the structure of hippocampal subfields is governed by shared genetic factors that differ along anterior-posterior axis but are shared among subfields [65–67]. Diffusion map embedding [68] was used to describe the gradients with the largest axes of variance in functional connectivity and microstructural covariance [25,35]. The twin set-up of the HCP data enabled us to quantify both the heritability of these intrinsic functional and microstructural representations, as well as the genetic coupling between hippocampal and isocortical microstructural profiles. Last, we studied the shared organisation of hippocampal function and structure to describe spatial co-variation of structure-function associations along genetic hippocampal organisational axes. We performed extensive robustness analysis to assess the stability of our findings. Overall, these analyses will help to further understand the relationship between the genetic basis of hippocampal organisation and its flexible functional role.

Results

Hippocampal-isocortical functional connectivity is heritable (Figure 1).

Hippocampal subfields i.e. subiculum (SUB), CA1-3 (CA), and CA4-DG (DG), were delineated automatically using SurfPatch, a previously validated surface-based subfield segmentation algorithm [69] (**Fig. 1A**). Resting-state (rs) fMRI time series were extracted along subfield surfaces and isocortical parcels (Glasser Atlas of 360 areas [70]) and correlated to estimate functional connectivity (FC). After quality assessment (**Fig. S1A**), n = 709 participants (395 women, mean ± SD age = 28.7 ± 3.7 y, 176 monozygotic twins, 178 siblings without twin status and 355 participants without familial relatedness, HCP S900 data release [62]) were included.

Hippocampal time series were averaged along each subfield (SUB: 1200 × 1, CA: 1200 × 1 and DG: 1200 × 1) and correlated with the isocortical time series (360 × 1200) for each subject. The resulting subfield-to-cortex FC measures (360 × 1) were labeled to the conte69 surface [71]. Subfield-isocortical FC measures were mapped using linear and mixed effects models in BrainStat and thresholded at t > 20 to indicate highest connections (https://github.com/MICA-MNI/BrainStat [72]) (**Fig. 1B**). Though overall patterns look similar across subfields, comparing connectivity we found each subfield to also have unique connectivity patterns (***Supplementary Material***). The strongest connections were found in the default-mode, somatomotor, visual and limbic areas, across subfields. To evaluate the heritability of isocortical FC, we ran SOLAR (Sequential Oligogenic Linkage Analysis Routines, SOLAR, v8.5.1) [73] heritability analysis on the mean subfield-to-isocortex FC measures (360 × 1) for every isocortical vertex across all subjects (n = 709) (**Fig. 1C**). Heritability scores (h^2) indicated that heritability of SUB-isocortex FC was the highest in regions part of sensorimotor (mean h^2 score: $\overline{h^2} = 0.31$) and default mode ($\overline{h^2} = 0.29$) networks (**Fig. S1B**). A similar heritability profile was observed for CA-isocortex FC, with highest heritability in sensorimotor ($\overline{h^2} = 0.36$), default mode ($\overline{h^2} = 0.31$) and dorsal attention ($\overline{h^2} = 0.30$) networks. For the DG-isocortex FC, compared to SUB and CA, we observed a higher heritability in the sensorimotor ($\overline{h^2} = 0.40$) and ventral attention ($\overline{h^2} = 0.29$) networks. The significance level of the h^2 scores were assessed using a likelihood ratio test (p-values) and then corrected for multiple comparisons using FDR (pFDR) (**Fig. 1D**). Throughout most of the cortical parcels, the

heritability was found to be significant, with an increasing number of significant parcels from SUB towards CA and DG.

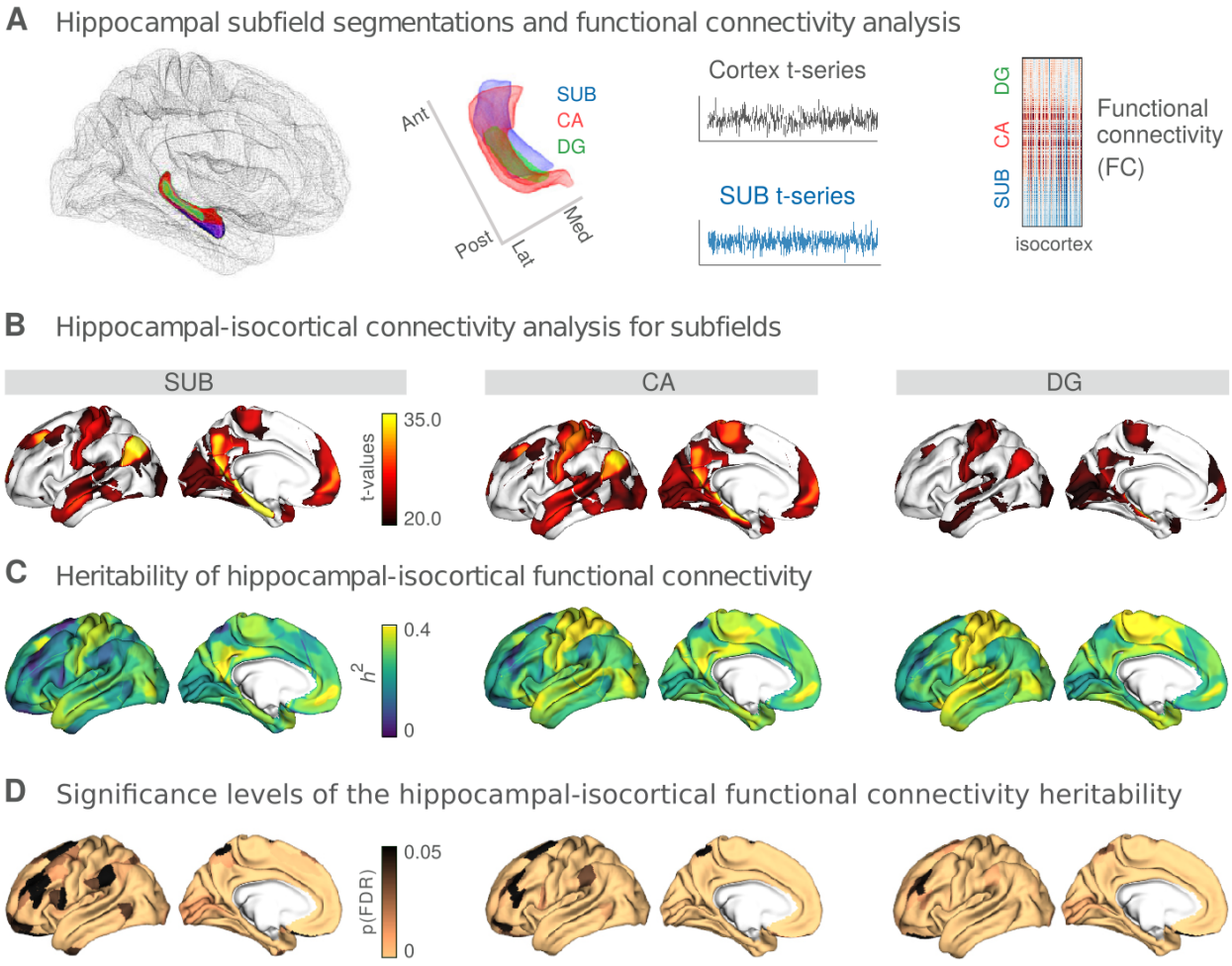

Fig. 1. Hippocampal-isocortical functional connectivity and its heritability. A. Hippocampal subfield surfaces were automatically delineated using SurfPatch [69]: subiculum (SUB, blue), CA1-3 (CA, red), and CA4-DG (DG, green). rs-fMRI time series were extracted along the individual subfields and correlated with the time series of the isocortex to obtain the functional connectivity (FC). **B.** Isocortex-wide FC of SUB (left), CA (middle), and DG (right). Isocortex-wide findings were thresholded at $t > 20$ to represent the highest connections. **C.** Heritability (h^2) scores of the subfield-isocortical functional couplings throughout the cortex. **D.** Significance levels of the h^2 scores from panel C. Significance level was reported with the multiple comparison corrected p-values (p(FDR)). Copper colour denotes pFDR < 0.05 and black colour pFDR ≥ 0.05.

Hippocampal functional organisation is moderately heritable (Figure 2).

Previous studies have reported strong heritability in hippocampal subfield volumes [74–76] (**Supplementary Table T4**). Here, we aimed to evaluate whether the functional organisation within hippocampal subfields was heritable as well. To do so, we first constructed topographic gradients of the hippocampal FC patterns using unsupervised dimension reduction [35,68] (**Fig. 2A**). Replicating previous work [35], the principal subfield gradient ($G1_{FC}$) presented an A-P axis across hippocampal subfields and explained 42.6% of the variance, whereas the second subfield gradient ($G2_{FC}$) described a M-L axis and explained 15.4% of the variance (**Fig. S2A**). Anterior hippocampal subfield portions (blue in **Fig. 2A**) were functionally coupled to sensorimotor, default mode and limbic networks (**Fig. 2B, Fig. S2B**). Posterior hippocampal subfield portions (yellow in **Fig. 2A**) were functionally more connected to fronto-parietal, salience, dorsal attention and visual networks (**Fig. 2B, Fig. S2B**).

Next, we computed the hippocampal-isocortical FC-heritability (h^2_{FC}) for every subfield vertex and then decomposed the FC-heritability onto its gradients ($G1(h^2_{FC})$) and $G2(h^2_{FC})$) (**Fig. 2C**). Performing the gradient decomposition on the FC-heritability, we aimed to probe a potential organisational axis underlying the heritability patterns of hippocampal-isocortical FC. The principal heritability gradient, $G1(h^2_{FC})$, depicted an A-P trajectory in h^2_{FC} profiles for all the subfields. We observed almost identical organisational axes stretching from anterior to posterior subfield portions for $G1_{FC}$ (**Fig. 2A**) and $G1(h^2_{FC})$ (**Fig. 2C**), although their gradient score loadings were different. However, the secondary heritability gradient, $G2(h^2_{FC})$, traversed the M-L axis for SUB, similar to $G2_{FC}$, but did not reveal a clear pattern for CA and DG.

We further obtained the heritability of the A-P and M-L functional gradients ($G1_{FC}$ and $G2_{FC}$) themselves, as represented in **Fig. 2A**, $h^2(G1_{FC})$ and $h^2(G2_{FC})$, respectively, to assess whether individual variations in local gradient loadings were heritable (**Fig. 2D**). For all subfields $h^2(G1_{FC})$ was found to be modest to low (SUB: mean: 0.14, range: [0, 0.29]; CA: mean: 0.08, range: [0, 0.32]; DG mean: 0.05, range: [0, 0.27]). Also the second gradient's heritability, $h^2(G2_{FC})$, was found to be modest to low for all subfields (SUB: mean: 0.09, range: [0, 0.30], CA: mean: 0.06, range: [0, 0.39], and DG: mean: 0.06, range: [0, 0.23]). Moreover, the heritability strength of both functional gradients did not show a clear spatial pattern (**Fig. S2C**).

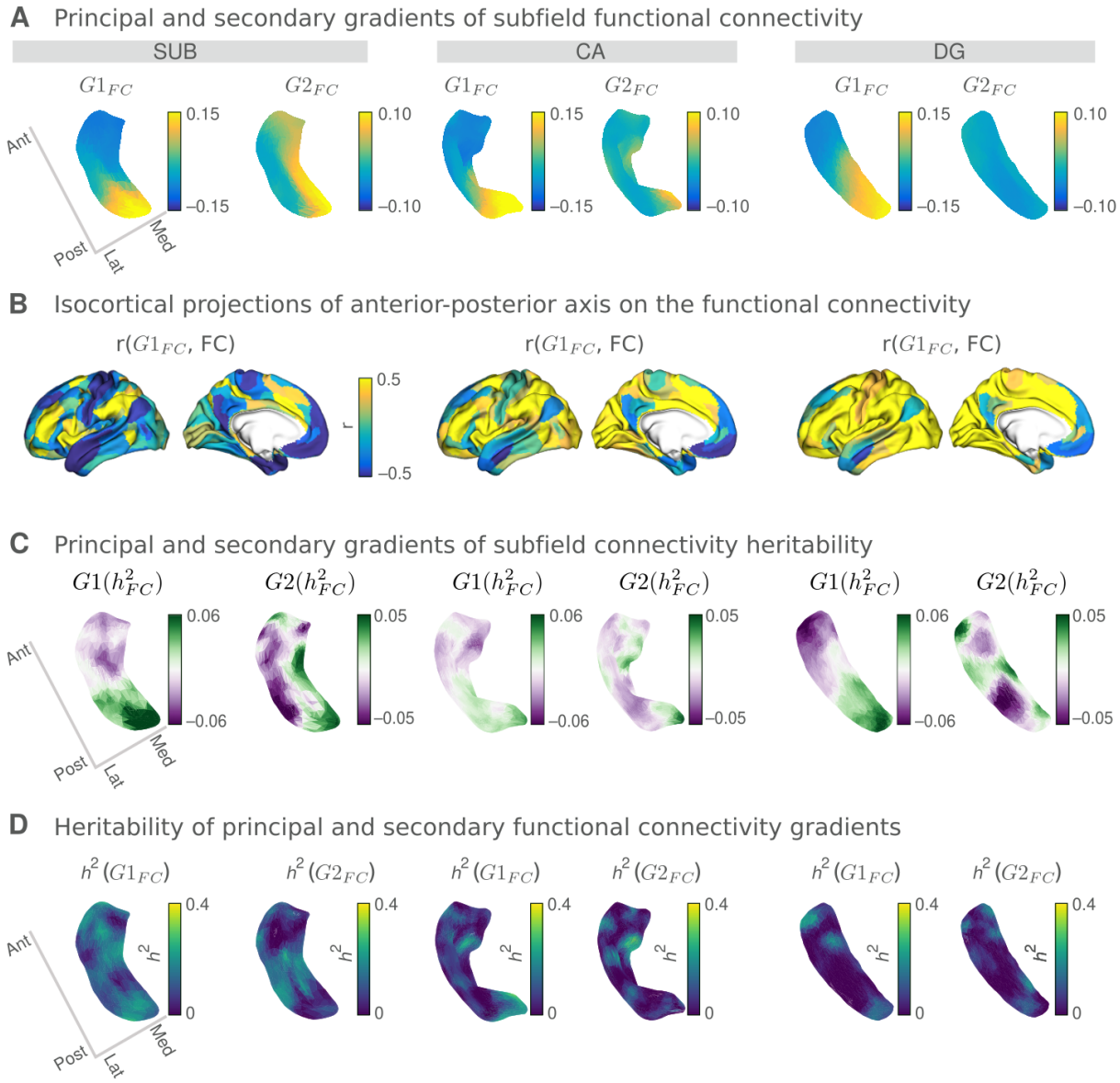

Fig. 2. Topological representations of hippocampal functional organisation and their heritability. A. Connectivity gradients of subfield-isocortical FC for SUB (left), CA (middle) and DG (right). Gradient 1 ($G1_{FC}$) depicts an anterior-posterior (A-P) connectivity axis, whereas Gradient 2 ($G2_{FC}$) displays a medial-lateral axis. **B.** Variations in hippocampal-isocortical FC across the $G1_{FC}$ projected on the isocortex (Pearson's r-values). Lower r-values (blue) indicate FC similarity between the anterior subfield portions and isocortex, whereas higher r-values (yellow) that of the posterior subfield portions and isocortex. **C.** Subfield-isocortical FC-heritability decomposed into its gradient representations. Primary gradient of FC-heritability $G1(h^2_{FC})$ depicts an A-P separation of the h^2 profiles for all subfields. **D.** Heritability of primary and secondary functional gradient loadings ($h^2(G1_{FC})$ and $h^2(G2_{FC})$) for each subfield vertex. Heritability analysis was run on $G1_{FC}$ and $G2_{FC}$ from Panel A and revealed a h^2 score for gradient loadings for each vertex.

Hippocampal microstructure is highly heritable and shows genetic correlation with the isocortex along its intrinsic organisational axes (Figure 3)

Having shown that functional connectivity of hippocampal subfields is heritable, but intrinsic functional organisation of subfields is less so, we aimed to evaluate the heritability of hippocampal subfield structure. To do so, we utilized individual T1w/T2w intensity maps to probe microstructure *in vivo* (**Fig. S3**). Local T1w/T2w maps were highly heritable across all subfields, reaching up to h^2 = 0.77 for SUB (mean ± SD = 0.44 ± 0.15 for SUB, 0.41 ± 0.12 for CA, and 0.43 ± 0.07 for DG) (**Fig. 3A**). Multiple comparison corrections using FDR reported significant heritability scores across almost all subfield vertices. By adjusting for the mean T1w/T2w as a covariate in the heritability model, we found similar heritability patterns for individual subfields, and both hemispheres (**Fig. S4).** This indicates that the heritability of subfields was present beyond any mean T1w/T2w intensity variation across individuals.

To evaluate the spatial similarity between local microstructure and functional gradients, we quantified the group-level association between the T1w/T2w and $G2_{FC}$ for subfields (**Fig. S5A**). T1w/T2w maps had the highest correlation with $G2_{FC}$ for the SUB (Pearson's r = 0.93, p-value after spatial autocorrelation correction [77]; p_{vario} < 0.001), and less with the other subfields (CA: r = 0.23, p_{vario} = 0.02, DG: r = -0.01, p_{vario} = 0.9). Furthermore, individual-level T1w/T2w and $G2_{FC}$ correlations were found to be significantly positive across participants for SUB (median $\bar{r}$ = 0.72, p < 0.005, one-tailed Wilcoxon signed-rank test) and CA ($\bar{r}$ = 0.22, p < 0.005), however not for DG ($\bar{r}$ = -0.04, p < 0.005) (**Fig. S5B**). We also computed the heritability of individual-level correlations (r (T1w/T2w, $G2_{FC}$)) and found them marginally heritable in SUB and CA but not DG (SUB: h^2 = 0.15 and p = 0.030, CA: h^2 = 0.15 and p = 0.011, DG: h^2 = 0 and p = 0.5). We further quantified the group-level association between the T1w/T2w and $G1_{FC}$ (**Fig. S5C**), that did not result in high associations (SUB: r = 0.20 and p_{vario} = 0.15, CA: r = 0.12 and p_{vario} = 0.19, DG: r = 0.37 and p_{vario} = 0.003). Last, we evaluated whether functional or microtructural axes of hippocampal formation was influenced by age and sex differences (**Fig. S6, S7**). Age and sex effects were both observed to be signficant along the subfield T1w/T2w measures, whereas age factor alone was reported to affect subfield FC measures more predominantly compared to the sex effects.

Then, we evaluated whether there is a genetic correlation between microstructure of hippocampal subfields and that of the isocortex, to probe whether potential co-variation of hippocampal and isocortical microstructure is governed by shared genetic factors. We first correlated vertex-wise subfield and parcel-wise isocortical T1w/T2w maps across all participants (n = 709), resulting in a structural intensity covariance (SiC) matrix (**Fig. 3B**). Using gradient decomposition, we evaluated intrinsic axes of covariance/genetic correlation within subfields based on their correspondence with isocortical microstructure [78]. The principal gradient of SiC ($G1_{SiC}$) revealed an A-P organisational axis across all the subfields **(Fig. 3C)**. We observed a high similarity between $G1_{SiC}$ and $G1_{FC}$ profiles (SUB: r = 0.88, CA: r =0.86, and DG: r =0.88, p_{vario}< 0.001 for all subfields). The second gradient of SiC ($G2_{SiC}$) did not represent a converging organisational pattern for the subfields. Evaluating the pattern of correlation between subfield-isocortex SiC and $G1_{SiC}$, we could assess how hippocampal and isocortical regions spatially relate to each other in terms of their microstructural similarity (**Fig. 3D**). Anterior hippocampal portions (blue in **Fig. 3C**) shared more microstructural similarity with the anterior isocortex, in particular anterior frontal and temporal cortex, while the posterior hippocampal portions (yellow in **Fig. 3C**) were related to visual cortex, lingual and fusiform areas, and sensorimotor cortex for SUB, and visual cortex, lingual and fusiform areas for CA. For the DG, we observed less divergent patterns of subfield-isocortical similarity between its anterior and posterior portions, with anterior portions relating to all of the isocortex except for visual, lingual and fusiform areas which showed a positive relation to posterior parts of DG.

Given that the hippocampal microstructure is highly heritable and shows heritable functional connectivity with the isocortex, we next evaluated whether hippocampal and isocortical microstructure are governed by shared genetic factors. Therefore, we computed genetic correlations (GEN) of the SiC between hippocampus and isocortex [79]. Here, assigning the SiC as our phenotype of interest, GEN analysis aimed to identify shared genetic processes underlying the microstructural similarity of hippocampus and isocortex. A high GEN score indicates that the microstructural phenotype of subfield and isocortex are influenced by the same set of genes [80]. Performing a gradient decomposition on the GEN measures, we observed highly similar gradients as in the SiC (**Fig. 3E**). The principal gradient of the GEN ($G1_{GEN}$) again displayed an A-P axis for all the subfields (**Fig. 3E**). Also $G1_{GEN}$ showed spatial similarity with $G1_{FC}$ (SUB: r = 0.67,

CA: r = 0.41, DG: r = 0.75, and p_{vario}< 0.001 for all subfields). The second gradient ($G2_{GEN}$) did not reveal a consistent organisational axis within each subfield, but rather varied between subfields. Analogous to SiC, we then investigated the correlation between hippocampal-isocortical GEN variations and $G1_{GEN}$ (**Fig. 3F**). Indeed, patterns were largely mirroring those observed in SiC, indicating that the structural intensity covariance between hippocampus and isocortex is largely concordant with genetic patterning.

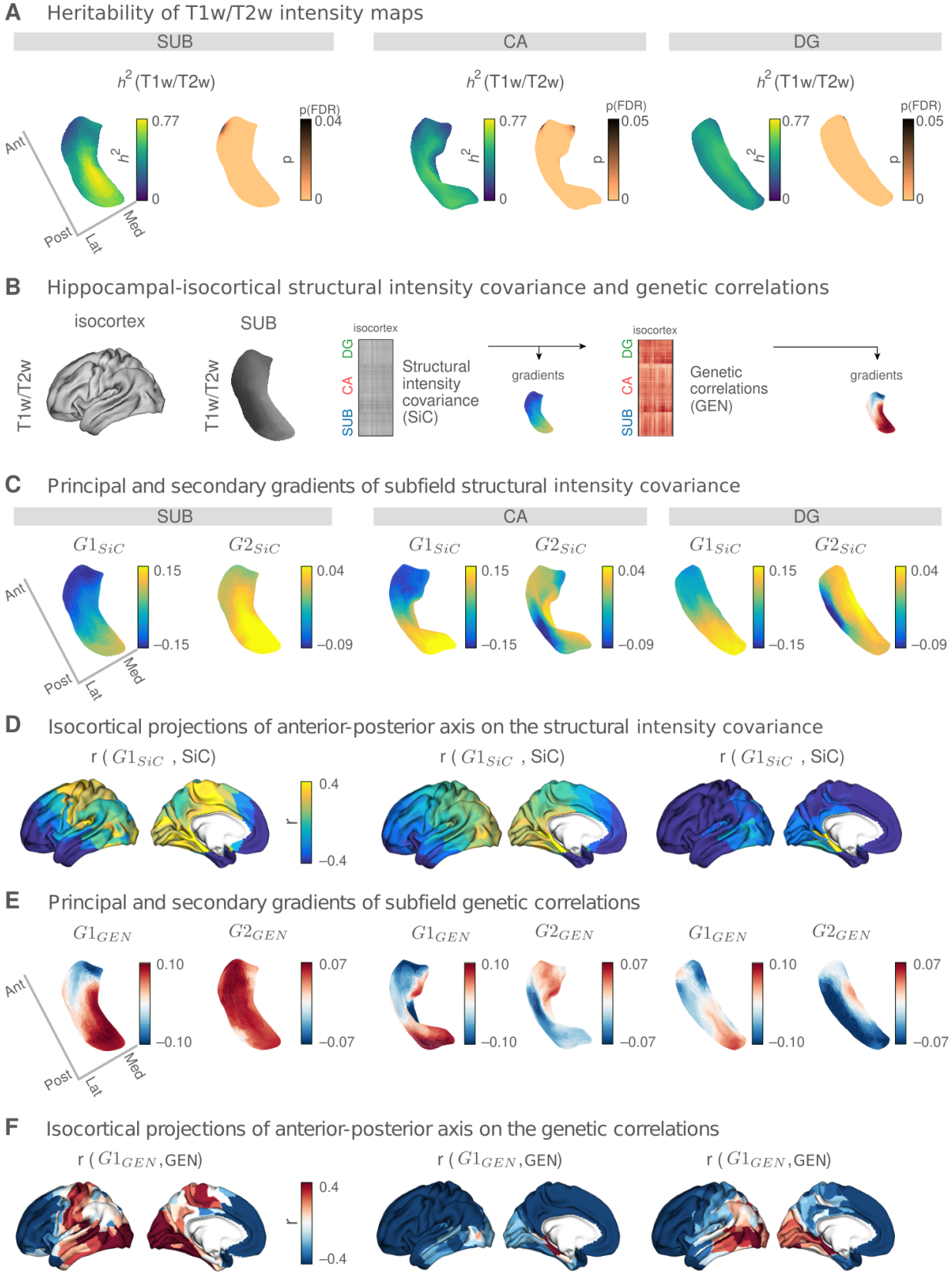
A Heritability of T1w/T2w intensity maps
SUB
CA
DG
h2 (T1w/T2w)
h2 (T1w/T2w)
h2 (T1w/T2w)
Ant
Post
Lat
Med
h2
0.77
0
p(FDR)
0.04
p
0
p(FDR)
0.05
B Hippocampal-isocortical structural intensity covariance and genetic correlations
isocortex
SUB
T1w/T2w
T1w/T2w
isocortex
DG
CA
SUB
Structural intensity covariance (SiC)
gradients
isocortex
Genetic correlations (GEN)
gradients
C Principal and secondary gradients of subfield structural intensity covariance
SUB
CA
DG
G1SiC
G2SiC
0.15
−0.15
0.04
−0.09
D Isocortical projections of anterior-posterior axis on the structural intensity covariance
r (G1SiC , SiC)
r
0.4
−0.4
E Principal and secondary gradients of subfield genetic correlations
G1GEN
G2GEN
0.10
−0.10
0.07
−0.07
F Isocortical projections of anterior-posterior axis on the genetic correlations
r (G1GEN,GEN)

Fig. 3. Hippocampal microstructural organisation and its heritability. A. Heritability of subfield T1w/T2w profiles (h^2(T1w/T2w)) and its significance levels. T1w/T2w maps were strongly heritable across all subfields. p-values were reported after multiple comparison corrections using FDR (copper colour denotes pFDR < 0.05, black pFDR > 0.05). **B.** Hippocampal-isocortical structural intensity covariance (SiC) was assessed by correlating hippocampal and isocortical T1w/T2w intensity maps across participants and subfields. Shared genetic variations in T1w/T2w intensity maps were assessed by conducting a genetic correlation (GEN) analysis on the SiC. Both SiC and GEN matrices were then decomposed into their gradient representations, separately. **C.** Gradients of SiC for SUB (left), CA (middle), and DG (right). $G1_{SiC}$ represents an anterior-posterior (A-P) axis for all subfields, whereas $G2_{SiC}$ reflects the differential axis of local transitions for individual subfields. **D.** Variations in SiC across its $G1_{SiC}$ projected on the isocortex (Pearson's r-values). Lower r-values (blue) indicate SiC similarity between the anterior subfield portions and isocortex, whereas higher r-values (yellow) that of the posterior subfield portions and isocortex. **E.** Gradients of GEN for SUB (left), CA (middle), and DG (right). $G1_{GEN}$ represents an A-P axis for all subfields, whereas $G2_{GEN}$ reflects the differential axis of local transitions for individual subfields. **F.** Variations in GEN across its $G1_{GEN}$ projected on the isocortex (Pearson's r-values). Lower r-values (dark blue) depict shared genetic influence between anterior subfield portions and isocortex and higher r-values (red) that of posterior subfield portions and isocortex.

Coupling of hippocampal subfield function and microstructure (Figure 4).

Last, we studied the shared organisation of hippocampal function and structure to evaluate whether regions with similar microstructure in hippocampus and isocortex also show a functional connection as predicted by the structural model. To do so, we computed the coupling of microstructure covariance and functional connectivity between the subfield and isocortex at each vertex of the subfields. Second, to probe whether the similarity of microstructure and functional profiles varied along the respective subfields' intrinsic functional and structural axes, we computed the degree of hippocampal organisational axes' similarity using the coefficient of determination (R^2) (**Fig. 4**). For SUB, we found a dominant pattern of A-P axes shared by $G1_{FC}$, $G1_{SiC}$, $G1_{GEN}$ and $G2_{SiC}$. However, the M-L axes, reflecting variation in local T1w/T2w and $G2_{FC}$, best described the coupling between microstructure and function (R^2 = 0.35), with lateral regions showing moderately positive coupling and medial regions showing low coupling. For CA, coupling rather followed a posterior (high) to anterior (low) pattern, corresponding to $G1_{FC}$, $G1_{SiC}$, $G1_{GEN}$ and $G2_{GEN}$ ($0.33 < R^2 < 0.64$). Last, for DG we found moderate variation in coupling, which showed a spatial relation to $G1_{FC}$, $G1_{SiC}$, $G1_{GEN}$ and $G2_{GEN}$($0.30 < R^2 < 0.49$). Here, posterior regions showing increased and anterior regions showing decreased coupling between microstructure covariance and functional connectivity.

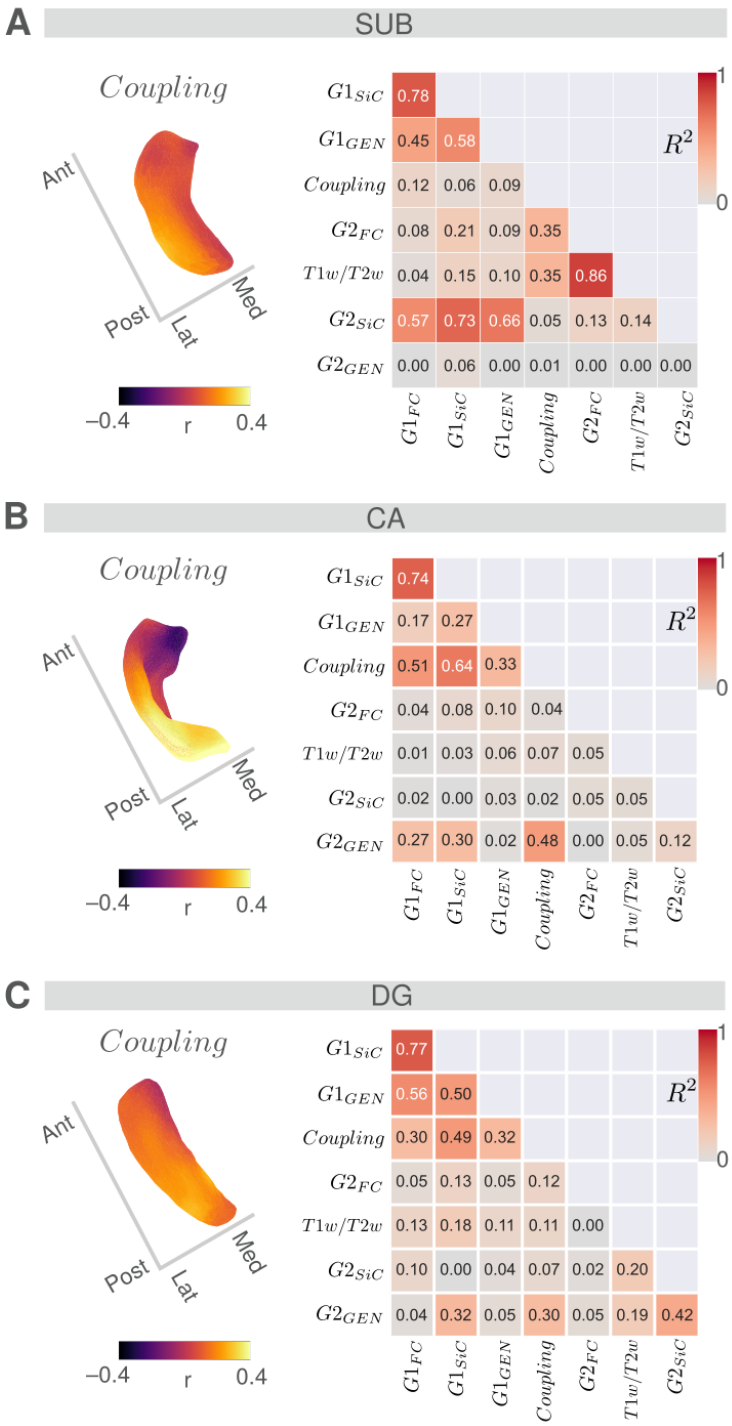

Fig. 4. Hippocampal structural-functional coupling maps and associations among organisational axes. A. SUB: Subfield vertex-wise coupling map between hippocampal-isocortical functional connectivity (FC) and structural intensity covariance (SiC) (upper panel). Higher coupling values (Pearson's r) denote an association between FC and SiC, whereas lower coupling values display a dissociation between them. Spatial similarity between hippocampal organisational axes ($G1 - G2_{FC}$, $G1 - G2_{SiC}$, $G1 - G2_{GEN}$, coupling and T1w/T2w maps) is denoted by the coefficient of determination R^2. High R^2 values (red) indicate a strong spatial alignment between the organisational axes, whereas low

R^2 values (grey) an unalignment. Panels **B.** and **C.** display coupling maps and R^2 values for **CA** and **DG**, respectively.

Discussion

The hippocampus is a densely interconnected region where stability and plasticity coincide. Building on emerging work describing the coalescence of anterior-to-posterior and medial-to-lateral gradients of function and microstructure in the hippocampal formation *in vivo* [21,35,81,82], we describe the heritability of hippocampal functional and structural organisation as well as its genetic relationship with the isocortex. First, we found that functional connectivity of hippocampal subfields to isocortex was heritable. However, intrinsic functional organisation of hippocampal subfields showed only marginal heritability. At the same time, we found that spatial variations in subfield T1w/T2w intensity maps, serving as a marker for myelin-related microstructure [63], were heritable and topographically related to local subfield functional organisation. Exploring the covariance of local hippocampal and isocortex microstructure, we found they consistently followed an A-P axis, with anterior subfield regions relating to anterior frontal and temporal cortex, whereas posterior subfield regions relating to visual and inferior temporal areas. These patterns were genetically correlated, indicating that microstructure of the subfields underlie shared genetic influences with the isocortex. Last, evaluating the similarity by the structure-function coupling in the hippocampal subfields along intrinsic hippocampal axes, we found lateral/posterior regions to be highly coupled, whereas anterior/medial regions were uncoupled. This illustrates how genetic axes may scaffold hippocampal structure and function, enabling a decoupling of function from structure in particular in anterior/medial areas, genetically linked to anterior/transmodal portions of the isocortex.

To study the heritability of subregional functional and microstructural organisation of the hippocampal formation, we automatically segmented the hippocampal formation via a subfield and surface-based approach (SUB, CA, and DG) [69], which has been previously validated in both healthy individuals and those with hippocampal pathology [11]. Such surface-based approaches improve anatomical alignment across individuals [81]. In the current work, we could replicate previously established hippocampal-cortical FC organisation across subfields. To preserve within-subfield interactions, we implemented the gradients approach on an across-all-subfields functional connectome (FC). This way, we obtained low-dimensional representations of hippocampal connectivity gradients in a purely connectome-driven and continuous fashion. Although

connectome gradients were obtained across-all-subfields once, they still represented subfield variations. For instance, the primary gradient emphasized A-P transitions (long axis [22,83–85]) in all subfields, whereas the secondary gradient depicted M-L separations (transverse axis [21,27,86]) predominantly for SUB, and indeed not for CA and DG. Also, the gradient decomposition of the FC-heritability itself delivered A-P profiles across all the subfields that highly resemble the A-P distribution of molecular hippocampal gradients as shown by [87]. Second, as in previous work, the M-L axis was found to align strongly with the microstructural proxy, particularly for the SUB and to a lesser extent in CA. In sum, we could replicate previous work [35] and again observe that specialisation of the long axis was preserved in all subfields, whereas the transverse axis indicated a link between intrinsic FC and microstructure, particularly in SUB.

Extending previous work describing mean axes of microstructural and functional organisation of hippocampal subfields, we investigated whether individual variation in hippocampal organisation was partly attributable to genetic factors. Previous molecular genetics studies have shown that hippocampal subregions as well as whole-hippocampal volumes exhibit strong heritability [88–90]. Moreover, genome-wide studies identified single-nucleotide polymorphisms (SNP) associated with hippocampal volumes [91–94] showing, in part, unique SNPs for each subfield and furthermore associated with neuropathology of schizophrenia [95,96]. Here, we extended this work by studying the heritability of subtle variations of microstructure and function within subfield surfaces, as well as their link to the isocortex. We observed highest heritability within the subfield microstructure proxy (T1w/T2w) and lowest for the A-P and M-L functional hippocampal gradients. Indeed, the heritability of both functional gradients was moderate to low, indicating that individual variation within functional gradients did not vary strongly as a function of genetic proximity of individuals. The variance explained by the functional gradient along the M-L axis, although they are topographically meaningful, was fairly low. This could reduce the ability to detect a significant heritability. At the same time, we found that heritability of subfield-isocortical FC was again organised along an A-P axis, indicating that anterior and posterior portions of hippocampal subfields have distinct and heritable relations with the isocortex. Moreover, we found that the functional M-L gradient correlated strongly with T1w/T2w microstructure along the hippocampal subfield surfaces, which, in turn, was highly heritable. It is possible that the intrinsic, heritable, structural axes within the hippocampus scaffold a more flexible functional organisation. Indeed,

environmentally induced brain changes may be interpreted as a degree of aberration from the heritability, i.e. the less heritable a brain region/metric, the larger the potential environmental influence [97–99]. It is thus possible that the low heritability of functional organisation of subfields reflects these variations, attributable to environmental effects and associated with hippocampal plasticity.

T1w/T2w intensity measures require careful consideration while interpreting the microstructure. T1w/T2w is a proxy for the myelination degree rather than being a direct biomarker for the cortical microstructure. However, although a direct relationship between cortical myelin and T1w/T2w measures has not yet been fully explained, there is subtle evidence for the T1w/T2w intensity revealing the myelin differentiation [100–103]. Of note, the T1w/T2w intensity also reflects the iron- and water-density, cytological variations such as dendritic arborization, cell size and cell density [104–106]. Previous work examining the gradients of the microstructural profile covariances built upon T1w/T2w measures showed that 1) the T1w/T2w intensity contrasts follow an A-P topography embedded in the cortex [107], and 2) this topography resembles a differentiation of mean myelin content from sensory towards fronto-polar areas [108]. Also, the T1w/T2w values were shown to follow R1 changes in HCP S900 sample [109], which is the inverse of quantitative T1 relaxation times (R1 = 1/qT1) and were furthermore projected in a difference dataset including healthy controls and epilepsy patients to explain the association between microstructural damage and a neuropathology [110].

Overall, our observations on heritability of functional and structural axes, functional connectivity with the cortex and genetic correlation between hippocampal microstructure and isocortical structure illustrate how genetic factors organize the hippocampal formation and association with the cortex at the level of the individual. Heritability is the proportion of variance in a population of a trait explained by inherited genetic variants. It is a measure that provides an estimate of the upper limit of how well we can predict a trait based on the genetic profile of an individual. As such the measurement of heritability provides a first estimate to what extent genetic and environmental factors may impact a given trait. Importantly, heritability is a feature of the population and not of an individual. Moreover, heritability is reduced when there is measurement error, but also as a function of non-genetic factors impacting variation across individuals. Consequently, the observed

reduced heritability of hippocampal functional organization may not mean that the hippocampus is under low genetic control per se. Rather it means that individual differences in functional gradients may be largely explained by non-genetic factors, such as variations of cognitive state, stress-levels or neuroendocrine levels [111,112]. Recent work in functional connectomics has indicated that the intrinsic FC in the isocortex may reflect more trait-like than state-like features [113]. Nevertheless, it is still possible that the captured variability in hippocampal functional organization may reflect more state-like features, also taking into account that the hippocampus is a region that is considered particularly plastic [114]. Next to effects on cognitive state on hippocampal function, hippocampal structure and function have been reported to be susceptible to variation hormonal status [115,116] and stress [117,118], factors that likely differ between twins at a given time point. In line with these observations, we found subtle co-variations between age and sex and hippocampal functional and structural organization [117,118], possibly suggestive of long-term hormonal plasticity effects as well as experience-driven plasticity effects. Future work may expand on our heritability analyses by studying in more detail how environmental factors may impact hippocampal organization in humans. For instance, feeding machine learning algorithms with heritability measures and hippocampal connecome gradients, a prediction of the behavioral capacity and therefore the individual differences could be possible. Also, evaluating the genetic impact on hippocampal dysregulation, we could understand hippocampus associated neuropathologies better. This would enhance detecting diseases at early stages and moreover suggest employing prophylactic treatments accordingly.

As the internal wiring of the hippocampus relates to its connectivity to the rest of the brain, we evaluated the genetic relationship between subfield surface microstructure and isocortical microstructure. To do so, we probed the covariance between hippocampal subfields and isocortex microstructure (structural intensity covariance, SiC), and their genetic correlation. SiC emphasizes the morphological similarity among brain regions, with high covariance between two regions across individuals indicating these regions share maturational and genetic trajectories [119]. Although the decomposed SiC and genetic correlation measure originated from the T1w/T2w maps, its low dimensional components depicted similar spatial organisation to that of the functional maps. The primary covariance gradient revealed an A-P axis for all the subfields, which was mirrored by a highly similar gradient based only on the genetic correlation between local subfield and isocortical

microstructure. This indicates a distinction between microstructure of anterior and posterior regions of hippocampal subfields based on its genetic similarity with the isocortex, which was found to be mirrored in its functional organisation in the current sample. Regions in anterior parts of the subfields showed a genetic similarity with anterior frontal and temporal cortex, whereas those in posterior parts of the subfields showed a genetic similarity with posterior occipital-temporal regions. Earlier studies have presented an isocortex-wide A-P topography derived from cortical thickness morphology [120], microstructural profile covariance [121], and grey matter volumes [25]. The isocortical A-P topography resembles a frontal-polar differentiation of myelin density [122,123] and shows spatial similarity with a cortical functional gradient traversing between the transmodal to unimodal axis [123,124]. In line with our observation that morphometric similarity of hippocampus and isocortex is genetically determined [125,126], the concordance of genetic similarity between the A-P subfield axis and A-P isocortical axis has been previously reported using transcriptomic data [127]. Thus, the internal, heritable, organisation of hippocampal subfield microstructure has a genetic correlation with isocortex, which spatially co-varies with its functional organisation.

Beyond similarities, we also observed differences in subfield-isocortical genetic associations, both in the primary and secondary covariance and genetic correlation gradient. For example, we found a clear differentiation between genetic relationships of hippocampus and isocortex along the anterior-posterior axes with posterior regions of CA, showing only little association with temporal-occipital regions, and SUB showing a clear distinction between anterior subfield regions and its correspondence to anterior frontal/temporal cortex and posterior subfield regions and its correspondence to temporo-occipital and sensory regions. Moreover, the second genetic correlation gradient varied strongly between SUB, CA, and DG, suggesting to vary rather as a function of subfield infolding. This may relate to the subfield specific neurodevelopmental trajectories. For example, the CA - Ammon's Horn - is one of the first brain regions to develop in the prenatal period [65,128]. Conversely, the SUB extends its maturation towards the postnatal period [129]. Finally, DG maturation exceeds the postnatal period [130], possibly underscoring posterior parietal associations. Thus, timing of pre- and post-natal development may be reflected in the genetic similarity patterning between subfields and their association with the isocortex. Non-genetic factors such as lifestyle impact the brain and behavior, also referred to as an experience-dependent plasticity in neuroanatomy [131]. Such factors may also modulate hippocampal structure

and functional development. For example, a recent study using genome-wide DNA methylation sequencing - a technique to mark gene activation patterns associated with cellular aging - showed that mice retained a 'younger' dentate gyrus under stimulating living conditions than those from low-stimulus environments [132]. A direct translation of animal findings on hippocampal neurogenesis is not possible, however, there has also been evidence for human hippocampal development affected by early-life experiences [133]. Chronic stress exposure in early childhood is linked to reduced hippocampal volume [134,135] and associated with behavioral deficits such as poor learning processes [136]. Detecting the T1w/T2w ratios in veterans, another study depicted a higher myelin content following posttraumatic stress disorder in young adults [137].

Lastly, to understand whether hippocampal function and structure covary along genetic organisational axes, we assessed local coupling maps of structural and functional subfield-isocortical profiles. Evaluating differences between structural and functional organisation, we found that coupling between structure and function was highest in posterior/medial portions of the hippocampal subfields, whereas anterior portions were uncoupled. Moreover, the coupling of hippocampal microstructure and function shows covariation with intrinsic functional and structural axes that we showed to align with genetic correlation to the isocortex. In particular, in the hippocampus, we found that posterior regions have a predominant structural and functional association with unimodal cortical regions whereas anterior regions are linked to transmodal cortex, similar to previous reports [82,127]. Thus, mirroring observations in the cortex [97,138], it may be that portions of the hippocampus associated with posterior/unimodal regions show more similarity between structure and function than those related to transmodal areas such as anterior frontal and temporal cortex. Functionally, the anterior hippocampus has been reported to participate in associative memory processing [139], in which DMN is also involved and known to be integrating with parietal and temporal lobes for episodic memory retrieval [140]. Conversely, the posterior hippocampus is suggested to be a mediator for spatial memory encoding [141], in which parietal cortices [142] and attention and salience networks are recruited [143]. Together, the divergence observed in function and structure along genetic axes of hippocampal subfields may reflect a hierarchy of complexity, with more uncoupled portions of the hippocampus enabling more flexible forms for cognitive processing, an important hypothesis for future studies to examine.

In sum, we showed that hippocampal subfields are organised along heritable posterior-to-anterior and medial-to-lateral axes which show a genetic link to isocortical functional and structural organisation. Though the current work focussed on functional organization described by gradient 1 and 2, together explaining 58% of eigenvariance in the functional connectome, future work may gain increased insights of hippocampal organization by studying also more subtle patterns crossing A-P and M-L axes. As another potential implication of gradients, one may evaluate the association between maturational axes in cortical structure and divergent functional profiles along the hippocampal formation. This may provide an important step to better understand how the anatomy of the hippocampus supports its unique and versatile function.

Materials and Methods

Participants

We leveraged the HCP S900 data release [144] with n = 898 subjects with resting-state fMRI sessions and high-resolution structural images. Participant recruitment procedures and informed consent forms, including consent to share de-identified data, were previously approved by the Washington University Institutional Review Board as part of the HCP. The current research complies with all relevant ethical regulations as set by The Independent Research Ethics Committee at the Medical Faculty of the Heinrich-Heine-University of Duesseldorf (study number 2018-317).

The quality assurance (QA) was based on the following exclusion criteria: ***i)*** subjects with anatomical anomalies or tissue segmentation errors listed in the HCP issues (n = 47), ***ii)*** subjects with missing four resting-state fMRI scan sessions (n = 69), ***iii)*** subjects with poor hippocampal subfield segmentation quality (n = 42), and ***iv)*** subjects whose functional connectome (FC) differed from the group level FC (n = 31), as a necessity for the gradient analysis (see section **Functional Connectivity and Gradients**). For the QA step ***iii)***, we first segmented hippocampal subfields: subiculum (**SUB**), CA1-3 (**CA**), and CA4-DG (**DG**) along the structural images using a patch-based surface algorithm (SurfPatch)[145]. Then, all subfield delineations underwent a visual inspection by Dr. Sofie Valk (SLV), Şeyma Bayrak (ŞB), and Reinder vos de Wael (RW). There remained n = 709 participants (395 women, mean ± SD age = 28.7 ± 3.7 y) accessible for our study. Among the 709 participants included in this study, there were 176 monozygotic twins, 178 siblings without twin status and 355 participants without familial relatedness. All QA steps and analysis scripts used in this study are available at https://github.com/CNG-LAB/cngopen/tree/main/hippocampus.

Neuroimaging Data Acquisition and Preprocessing

Details of the HCP neuroimaging protocol and processing pipelines are available at [146]. In brief, we extracted T1-weighted (T1w) and T2-weighted (T2w) images available in the HCP initiative, which were all acquired on a 3T Siemens Skyra scanner. T1w images were acquired using a three-dimensional magnetization prepared rapid gradient-echo (3D-MPRAGE) sequence (0.7 mm isotropic voxels, matrix = 320 × 320, 256 sagittal slices, TR = 2400 ms, TE = 2.14 ms, TI = 1000

ms, flip angle = 8°, iPAT = 2). Two T2w images were acquired with identical geometry (TR=3200 ms, TE=565 ms, variable flip angle; iPAT=2). Resting-state fMRI images were acquired using a multi-band accelerated 2D-BOLD echo-planar imaging (EPI) sequence (2 mm isotropic voxels, matrix = 104 × 90, 72 sagittal slices, TR = 720 ms, TE = 33 ms, flip angle = 52°, mb factor = 8, 1200 volumes/scan). The fMRI data was collected at two sessions (1, 2) and in two phase encoding directions at each session (left-right [LR] and right-left [RL]), resulting in four resting-state fMRI datasets in total ([LR1], [RL1], [LR2], [RL2]).

Preprocessing steps for the structural MRI images included gradient nonlinearity correction, brain extraction, distortion correction and co-registration of T1w and T2w images using rigid body transformations. Then, an intensity nonuniformity correction was performed using T1w and T2w contrasts [63] and subcortical structures were segmented using FSL FIRST [147]. Subsequently, preprocessed images were nonlinearly registered to the MNI152 template and cortical surfaces were reconstructed with FreeSurfer 5.3.0-HCP [148–150]. Finally, the individual cortical surfaces were registered to the Conte69 template [71] using MSMA11 [70].

Preprocessing of rs-fMRI images included corrections for the gradient nonlinearity, head motion and distortion. The images were then aligned to the T1w space using rigid-body and boundary-based registrations together [151]. The transformation matrices from this alignment step and that of the earlier T2w to T1w alignment were concatenated and applied to the rs-fMRI images at a single interpolation step to warp rs-fMRI images to the MNI152. Further processing in MNI152 space included bias field removal, whole brain intensity normalisation, high pass filtering (> 2000s FWHM) and noise removal with the ICA-FIX procedure [152].

Hippocampus Subfield Segmentations

We used the SurfPatch algorithm [153] to automatically delineate the hippocampal subfields of all participants: subiculum (SUB), CA1-3 (CA), and CA4-DG (DG). The automated delineation was carried out on the minimally processed T1w neuroimaging data in the MNI152 template space, using a validated multi-template surface-patch algorithm [69]. SurfPatch was previously trained on another brain dataset of a multi-contrast and sub-millimetric MRI data at 3 Tesla, which included manual hippocampal subfield delineations [154]. In previous work, [69] have reported the association

between accuracy and T1-image resolution. Overall, higher associations between manual and automated volumes are found based on sub-millimeter T1 as compared to millimeter level T1, yet differences in correlation are marginal [69]. Dice overlap between automated and manual segmentations were above 81.10 ± 3.86%. The current work used T1 maps with a resolution of 0.7 mm isotropic voxel, and projected functional maps of 2.0 mm isotropic voxel.

SurfPatch performs a spherical harmonic shape parametrization and point distribution model of the surfaces [155]. The medial sheet representations of hippocampal subfields were generated by running through each subfield's core using a Hamilton-Jacobi approach [156] to minimize partial volume effects due to feature sampling. Furthermore, the spherical harmonic parametrization was propagated from the outer shell to the medial sheet for a better match of vertex-correspondence across individuals based on shape-inherent information. Resultant CA surfaces consisted of 10242 vertices and both DG and SUB surfaces of 5762 vertices. Next, CA, DG, and SUB surfaces were further downsampled to 2048, 1024, and 1024 vertices, respectively. All subfield segmentations generated by the SurfPatch underwent a visual inspection and are available upon request. The visual inspection reports from the previously published vos de Wael et. al. 2018 were included for n = 399 subjects, and Dr. Sofie Valk (SLV) and Şeyma Bayrak (ŞB) inspected further the remaining n = 499 subjects in the S900 data release.

Isocortex and Subfield Time Series

We mapped medial sheet meshes and volumetric resting-state fMRI data to native T1w space. Time series were sampled at each hippocampal and cortical mid-thickness vertex [70]. Hippocampal surface features were smoothed using a Gaussian diffusion kernel with 5 mesh units as FWHM in all subfields and isocortex. Sampling was carried out in a native T1w space to minimize the interpolation. Cortical time series were averaged within a previously established multi-modal parcellation scheme of the Glasser Atlas of 360 areas (180 regions per hemisphere) [70]. Surface-based time series were smoothed using a Gaussian diffusion kernel with 5 mesh units as full-width-at-half-maximum (FWHM).

Functional Connectivity

For every participant separately (n = 740), we computed the linear correlation coefficients between isocortex-wide time series (360×1200) and hippocampal subfield time series for SUB (1024×1200), CA (2048×1200), and DG (1024×1200). This resulted in a isocortex wide functional connectivity (FC) map (360×1) for every subject and subfield. We obtained group-level reference FC maps for every subfield by averaging individual FC maps across participants. We further profiled the similarity of individual FC maps to the reference FC maps by means of simple correlation (**Fig. S1A**). Participants with a lower degree of similarity ($r < 0.45$) to the reference map were excluded (n = 31). Finally, the FC map of the isocortex to each hippocampal subfield for the remaining 709 participants was mapped using linear and mixed effects models in BrainStat (https://github.com/MICA-MNI/BrainStat).

T1w/T2w Maps and Structural Intensity Covariance

To study microstructural features of the hippocampus, we used the ratio of T1- over T2-weighted (T1w/T2w) image intensities. We resampled native T1w/T2w images to the MNI152 space and mapped them to hippocampal subfield surfaces (SUB, CA, DG) using Connectome Workbench (v1.4.2, volume-warpfield-resample and volume-to-surface-mapping tools) [157]. To assess the quality of T1w/T2w intensities projected on the hippocampal subfields, we obtained the mean T1w/T2w intensity distributions of all participants for potential outlier detection **(Fig. 2A, Fig. S3C)**. We computed the structural intensity covariance (SiC) by correlating hippocampal and cortical T1w/T2w intensity maps resulting in 1384×1384 matrix for SUB, 2408×2408 matrix for CA, and 1384×1384 matrix for DG.

Heritability and Genetic Correlation

Heritability and genetic correlation analysis were conducted with the Sequential Oligogenic Linkage Analysis Routines (SOLAR, v8.5.1, http://www.solar-eclipse-genetics.org/). SOLAR employs a maximum likelihood variance-decomposition approach optimised to perform genetic analyses in pedigrees of arbitrary size and complexity [79,158]. SOLAR models genetic proximity by covariance between family members [79,158].

In brief, heritability (i.e. narrow-sense heritability h^2) is defined as the proportion of the phenotypic variance (σ_p^2) in a trait that is attributable to the additive effects of genes (σ_g^2), i.e. $h^2 = \sigma_g^2/\sigma_p^2$. SOLAR estimates heritability by comparing the observed phenotypic covariance matrix with the covariance matrix predicted by kinship [79,158]. Significance of the heritability estimate was tested using a likelihood ratio test where the likelihood of a restricted model (with σ_g^2 constrained to zero) is compared with the likelihood of the estimated model. Twice the difference between the log likelihoods of these models yields a test statistic, which is asymptotically distributed as a 50:50 mixture of a χ^2 variable with 1 degree-of-freedom and a point mass at zero [79,158]. We quantified the heritability of (i) hippocampal-isocortical functional connectivity patterns, (ii) hippocampal subfield gradients, and (iii) T1w/T2w intensity maps. We included covariates in all heritability analyses including age, sex, $age \times sex$, $age^2$and $age^2 \times sex$. Quantitative variables are mean-adjusted in SOLAR, avoiding collinearity for age squared effects.

To estimate if variations in T1w/T2w intensity maps between hippocampus and isocortex were influenced by the same genetic factors, a genetic correlation analysis was conducted. Genetic correlations indicate the proportion of variance that determines the extent to which genetic influences on one trait are shared with genetic influences on another trait (e.g. pleiotropy). In SOLAR, the phenotypic correlation (ρ_p) was decomposed through bivariate polygenic analyses to estimate genetic (ρ_g) and environmental (ρ_e) correlations using the following formula: $\rho_p = \rho_g\sqrt{h_1^2 h_2^2} + \rho_e\sqrt{(1-h|1^2)(1-h_2^2)}$, where h_1^2 and h_2^2 are the heritability estimates of the vertex-based values in hippocampus and isocortex [80,159]. The significance of these correlations was determined (similar to heritability analyses) by likelihood ratio tests comparing a model in which ρ_g was estimated with a model in which ρ_g was constrained to zero (no shared genetic effect) and constrained to 1 (complete pleiotropy) [80,159].

Hippocampal-Isocortical Functional Connectivity Heritability

Hippocampal time series were averaged across subfield vertices, yielding mean time series for SUB : (1 × 1200), CA : (1 × 1200), and DG : (1 × 1200) and for every subject. The subfield mean time series were then correlated with that of the cortex (360 × 1200). This approach resulted in mean subfield-to-isocortex FC matrices (mean SUB-isocortex : (360 × 1), CA-isocortex: (360 × 1), DG-isocortex : (360 × 1)). Having saved the mean subfield-isocortical FC for every subject (n

= 709) and every cortical vertex (360), we ran SOLAR heritability analysis along Glasser vertices FC values (709 × 360). SOLAR runs the heritability analysis for each vertex by taking the familial relatedness (HCP pedigree files) into account, ie. whether an FC value of the given Glasser vertex is heritable. At the end, having the heritability scores for 360 Glasser parcels, we labeled them to conte69 template [71] for the cortex visualizations in **Fig. 1C**.

Connectivity Gradients

Using the diffusion embedding algorithm, we generated low-dimensional representations of hippocampal-cortical FC, namely the *gradients*. For every participant separately (n = 709), we computed the linear correlation coefficients between isocortex-wide time series 360 × 1200 and hippocampal subfield time series for SUB (1024 × 1200), CA (2048 × 1200), and DG (1024 × 1200) to identify the FC matrices. Subfield-to-isocortex FC measures were concatenated across the subfields, yielding a hippocampal-isocortical FC map (4096 × 360) for every subject. Averaging FC matrices across all subjects (n = 709), we obtained a group level FC matrix. We used BrainSpace [160,161] to derive connectivity gradients from the group-level FC matrix using diffusion map embedding (normalised angle kernel, 90th percentile thresholding for the sparsity, and diffusion time estimation of α = 0.5) [68], similarly to those identified by Vos de Wael (2018).

Along each single gradient (4096 × 1), hippocampus vertices that share similar connectivity patterns have similar embedding values. The first and second gradients explained 58% of the total variance in the subfield FC map (**Fig. S2A**). Having validated the gradient representations of hippocampal subfields at the group-level, we computed the individual-level gradients for every participant. Subsequently, individual gradients were aligned to the group-level gradients using Procrustes alignment to be scaled onto a common embedded connectivity space.

Gradients of Subfield Functional Connectome Heritability

To probe the organisational axis of heritability scores itself, we derived the gradient decomposition of FC-heritabilities along subfields. We computed *1)* the subfield-to-cortex FC matrix, *2)* the heritability of this FC matrix (h^2_{FC}), and *3)* the gradient decomposition of the FC-heritability ($G1(h^2_{FC})$ and $G2(h^2_{FC})$). FC was obtained for each subject (n = 709) and subfield (SUB-cortex : 1024 × 360, CA-cortex : 2048 × 360, and DG-cortex : 1024 × 360), separately. We ran SOLAR

heritability analysis for every FC value from every subfield vertex to cortical vertex, resulting in heritability of FC, (h^2_{FC}, for SUB : (1024 × 360), CA : (2048 × 360) and DG : (1024 × 360). We then concatenated these data arrays across subfields, that yielded a h^2_{FC} matrix of size (4096 × 360). This heritability matrix was then decomposed into its gradients, resulting in the primary and secondary gradients of FC-heritability, $G1(h^2_{FC})$) and $G2(h^2_{FC})$, respectively.

Structure-Function Coupling along Subfields

To measure "coupling", we evaluated the degree of spatial overlap between hippocampal microstructural intensity covariance (SiC) and functional connectivity (FC) measures per subfield vertex. The SiC was computed by correlating the T1w/T2w measures between hippocampus and cortex across all subjects, which yielded a covariance matrix of size (4096 × 360). The FC was computed by correlating the time series between hippocampus and cortex, which yielded a connectivity matrix of size (4096 × 360). For every subfield vertex, we obtained the SiC array from that vertex to all cortical vertices (360 × 1), and FC array from the same vertex to all cortical vertices (360 × 1). We then correlated these two arrays (Pearson's r) to quantify the degree of spatial overlap between the SiC and FC profiles. This degree of spatial overlap was then called as "coupling", ie. a higher coupling value indicates a high overlap between SiC and FC measures for a subfield vertex, whereas a low coupling (or "uncoupling") depicts a low overlap. Similar approaches have been used by [162,163].

Acknowledgements

We would like to thank the various contributors to the open access databases that our data was downloaded from. Funding: HCP data were provided by the Human Connectome Project, Washington University, the University of Minnesota, and Oxford University Consortium (Principal Investigators: David Van Essen and Kamil Ugurbil; 1U54MH091657) funded by the 16 NIH Institutes and Centers that support the NIH Blueprint for Neuroscience Research; and by the McDonnell Center for Systems Neuroscience at Washington University. This study was supported by the Deutsche Forschungsgemeinschaft (DFG, EI 816/21-1), the National Institute of Mental Health (R01-MH074457), the Helmholtz Portfolio Theme "Supercomputing and Modeling for the Human Brain" and the European Union's Horizon 2020 Research and Innovation Program under Grant Agreement No. 785907 (HBP SGA2). R.V. was supported by the Richard and Ann Sievers award. S.L.V. was supported by Max Planck Gesellschaft (Otto Hahn award). B.C.B. acknowledges support from the SickKids Foundation (NI17-039), the National Sciences and Engineering Research Council of Canada (NSERC; Discovery-1304413), CIHR (FDN154298), Azrieli Center for Autism Research (ACAR), an MNI-Cambridge collaboration grant, and the Canada Research Chairs program. Last, this work was funded in part by Helmholtz Association's Initiative and Networking Fund under the Helmholtz International Lab grant agreement InterLabs-0015, and the Canada First Research Excellence Fund (CFREF Competition 2, 2015-2016) awarded to the Healthy Brains, Healthy Lives initiative at McGill University, through the Helmholtz International BigBrain Analytics and Learning Laboratory (HIBALL). M.D.H. was funded by the Max Planck Society and the German Ministry of Education and Research.

Author contributions

Ş.B., and S.L.V. conceived and designed the analysis, performed the analysis, wrote the draft manuscript and revised the manuscript. R.V. and H.L.S. aided in data analysis. A.B., B.C., N.B, R.V., and B.C.B. provided hippocampal subfield segmentations. All authors helped with writing and revising the manuscript.

Competing interests

The authors declare no conflict of interest.

References

1. Battaglia, F. P., Benchenane, K., Sirota, A., Pennartz, C. M. A. & Wiener, S. I. The hippocampus: hub of brain network communication for memory. *Trends Cogn. Sci.* **15**, 310–318 (2011).
2. Milner, B., Squire, L. R. & Kandel, E. R. Cognitive Neuroscience and the Study of Memory. *Neuron* vol. 20 445–468 (1998).
3. Squire, L. R. Memory and the hippocampus: a synthesis from findings with rats, monkeys, and humans. *Psychol. Rev.* **99**, 195–231 (1992).
4. Burgess, N., Maguire, E. A. & O'Keefe, J. The human hippocampus and spatial and episodic memory. *Neuron* **35**, 625–641 (2002).
5. Phelps, E. A. Human emotion and memory: interactions of the amygdala and hippocampal complex. *Curr. Opin. Neurobiol.* **14**, 198–202 (2004).
6. Franklin, T. B., Saab, B. J. & Mansuy, I. M. Neural mechanisms of stress resilience and vulnerability. *Neuron* **75**, 747–761 (2012).
7. Pruessner, J. C. *et al.* Stress regulation in the central nervous system: evidence from structural and functional neuroimaging studies in human populations - 2008 Curt Richter Award Winner. *Psychoneuroendocrinology* **35**, 179–191 (2010).
8. Lupien, S. J., McEwen, B. S., Gunnar, M. R. & Heim, C. Effects of stress throughout the lifespan on the brain, behaviour and cognition. *Nat. Rev. Neurosci.* **10**, 434–445 (2009).
9. Lieberman, J. A. *et al.* Hippocampal dysfunction in the pathophysiology of schizophrenia: a selective review and hypothesis for early detection and intervention. *Molecular Psychiatry* vol. 23 1764–1772 (2018).
10. Karl, A. *et al.* A meta-analysis of structural brain abnormalities in PTSD. *Neuroscience & Biobehavioral Reviews* vol. 30 1004–1031 (2006).
11. Bernhardt, B. C. *et al.* The spectrum of structural and functional imaging abnormalities in temporal lobe epilepsy. *Ann. Neurol.* **80**, 142–153 (2016).
12. Iglesias, J. E. *et al.* A computational atlas of the hippocampal formation using ex vivo , ultra-high resolution MRI: Application to adaptive segmentation of in vivo MRI. *NeuroImage* vol. 115 117–137 (2015).
13. Palomero-Gallagher, N., Kedo, O., Mohlberg, H., Zilles, K. & Amunts, K. Multimodal mapping and analysis of the cyto- and receptorarchitecture of the human hippocampus. *Brain Struct. Funct.* **225**, 881–907 (2020).
14. Wisse, L. E. M. *et al. A Harmonized Segmentation Protocol for Hippocampal and Parahippocampal Subregions: Why Do We Need One and what are the Key Goals?* (2017).
15. Yushkevich, P. A. *et al.* Quantitative comparison of 21 protocols for labeling hippocampal subfields and parahippocampal subregions in in vivo MRI: towards a harmonized segmentation protocol. *Neuroimage* **111**, 526–541 (2015).
16. van Strien, N. M., Cappaert, N. L. M. & Witter, M. P. The anatomy of memory: an interactive overview of the parahippocampal-hippocampal network. *Nat. Rev. Neurosci.* **10**, 272–282 (2009).
17. de Flores, R. *et al.* Intrinsic connectivity of hippocampal subfields in normal elderly and mild cognitive impairment patients. *Hum. Brain Mapp.* **38**, 4922–4932 (2017).
18. Hodgetts, C. J. *et al.* Ultra-High-Field fMRI Reveals a Role for the Subiculum in Scene Perceptual Discrimination. *The Journal of Neuroscience* vol. 37 3150–3159 (2017).
19. Berron, D. *et al.* Strong Evidence for Pattern Separation in Human Dentate Gyrus.

J. Neurosci. **36**, 7569–7579 (2016).
20. Neunuebel, J. P. & Knierim, J. J. CA3 retrieves coherent representations from degraded input: direct evidence for CA3 pattern completion and dentate gyrus pattern separation. *Neuron* **81**, 416–427 (2014).
21. Plachti, A. *et al.* Multimodal Parcellations and Extensive Behavioral Profiling Tackling the Hippocampus Gradient. *Cereb. Cortex* **29**, 4595–4612 (2019).
22. Strange, B. A., Witter, M. P., Lein, E. S. & Moser, E. I. Functional organization of the hippocampal longitudinal axis. *Nat. Rev. Neurosci.* **15**, 655–669 (2014).
23. Bienkowski, M. S. *et al.* Integration of gene expression and brain-wide connectivity reveals the multiscale organization of mouse hippocampal networks. *Nat. Neurosci.* **21**, 1628–1643 (2018).
24. Cenquizca, L. A. & Swanson, L. W. Spatial organization of direct hippocampal field CA1 axonal projections to the rest of the cerebral cortex. *Brain Res. Rev.* **56**, 1–26 (2007).
25. Kharabian Masouleh, S., Plachti, A., Hoffstaedter, F., Eickhoff, S. & Genon, S. Characterizing the gradients of structural covariance in the human hippocampus. *Neuroimage* **218**, 116972 (2020).
26. Nordin, K. *et al.* Structural whole-brain covariance of the anterior and posterior hippocampus: Associations with age and memory. *Hippocampus* **28**, 151–163 (2018).
27. Maass, A., Berron, D., Libby, L. A., Ranganath, C. & Düzel, E. Functional subregions of the human entorhinal cortex. *Elife* **4**, (2015).
28. Margulies, D. S. *et al.* Situating the default-mode network along a principal gradient of macroscale cortical organization. *Proc. Natl. Acad. Sci. U. S. A.* **113**, 12574–12579 (2016).
29. Bayrak, Ş. *et al.* The impact of ischemic stroke on connectivity gradients. *Neuroimage Clin* **24**, 101947 (2019).
30. Langs, G. *et al.* Identifying Shared Brain Networks in Individuals by Decoupling Functional and Anatomical Variability. *Cereb. Cortex* **26**, 4004–4014 (2016).
31. Krienen, F. M. & Sherwood, C. C. Gradients of Connectivity in the Cerebral Cortex. *Trends in cognitive sciences* vol. 21 61–63 (2017).
32. Genon, S., Bernhardt, B. C., La Joie, R., Amunts, K. & Eickhoff, S. B. The many dimensions of human hippocampal organization and (dys)function. *Trends Neurosci.* **44**, 977–989 (2021).
33. Li, Q. *et al.* Human brain function during pattern separation follows hippocampal and neocortical connectivity gradients. doi:10.1101/2020.06.22.165290.
34. Przeździk, I., Faber, M., Fernández, G., Beckmann, C. F. & Haak, K. V. The functional organisation of the hippocampus along its long axis is gradual and predicts recollection. *Cortex* **119**, 324–335 (2019).
35. Vos de Wael, R. *et al.* Anatomical and microstructural determinants of hippocampal subfield functional connectome embedding. *Proc. Natl. Acad. Sci. U. S. A.* **115**, 10154–10159 (2018).
36. McEwen, B. S. Stress and hippocampal plasticity. *Annu. Rev. Neurosci.* **22**, 105–122 (1999).
37. Bannerman, D. M. *et al.* Hippocampal synaptic plasticity, spatial memory and anxiety. *Nat. Rev. Neurosci.* **15**, 181–192 (2014).
38. Whelan, C. D. *et al.* Heritability and reliability of automatically segmented human

hippocampal formation subregions. *Neuroimage* **128**, 125–137 (2016).
39. Elman, J. A. *et al.* Genetic architecture of hippocampal subfields on standard resolution MRI: How the parts relate to the whole. *Hum. Brain Mapp.* **40**, 1528–1540 (2019).
40. van der Meer, D. *et al.* Brain scans from 21,297 individuals reveal the genetic architecture of hippocampal subfield volumes. *Mol. Psychiatry* **25**, 3053–3065 (2020).
41. Zhao, B. *et al.* Heritability of Regional Brain Volumes in Large-Scale Neuroimaging and Genetic Studies. *Cereb. Cortex* **29**, 2904–2914 (2019).
42. Hibar, D. P. *et al.* Novel genetic loci associated with hippocampal volume. *Nat. Commun.* **8**, 13624 (2017).
43. Hibar, D. P. *et al.* Common genetic variants influence human subcortical brain structures. *Nature* **520**, 224–229 (2015).
44. Stein, J. L. *et al.* Identification of common variants associated with human hippocampal and intracranial volumes. *Nat. Genet.* **44**, 552–561 (2012).
45. Maller, J. J. *et al.* Hippocampal volumetrics in treatment-resistant depression and schizophrenia: the devil's in de-tail. *Hippocampus* **22**, 9–16 (2012).
46. Warland, A., Kendall, K. M., Rees, E., Kirov, G. & Caseras, X. Schizophrenia-associated genomic copy number variants and subcortical brain volumes in the UK Biobank. *Mol. Psychiatry* **25**, 854–862 (2020).
47. McEwen, B. S. Stress and hippocampal plasticity. *Annu. Rev. Neurosci.* **22**, 105–122 (1999).
48. Bannerman, D. M. *et al.* Hippocampal synaptic plasticity, spatial memory and anxiety. *Nat. Rev. Neurosci.* **15**, 181–192 (2014).
49. Barth, C. *et al.* In-vivo Dynamics of the Human Hippocampus across the Menstrual Cycle. *Sci. Rep.* **6**, 32833 (2016).
50. Zsido, R. G. *et al.* Longitudinal 7T MRI reveals volumetric changes in subregions of human medial temporal lobe to sex hormone fluctuations. doi:10.1101/2022.05.02.490281.
51. Kim, E. J., Pellman, B. & Kim, J. J. Stress effects on the hippocampus: a critical review. *Learning & Memory* vol. 22 411–416 (2015).
52. Barbas, H. General cortical and special prefrontal connections: principles from structure to function. *Annu. Rev. Neurosci.* **38**, 269–289 (2015).
53. Valk, S. L. *et al.* Genetic and phylogenetic uncoupling of structure and function in human transmodal cortex. doi:10.1101/2021.06.08.447522.
54. Suárez, L. E., Markello, R. D., Betzel, R. F. & Misic, B. Linking Structure and Function in Macroscale Brain Networks. *Trends Cogn. Sci.* **24**, 302–315 (2020).
55. Baum, G. L. *et al.* Development of structure-function coupling in human brain networks during youth. *Proc. Natl. Acad. Sci. U. S. A.* **117**, 771–778 (2020).
56. Paquola, C. *et al.* Microstructural and functional gradients are increasingly dissociated in transmodal cortices. *PLoS Biol.* **17**, e3000284 (2019).
57. Valk, S. L. *et al.* Genetic and phylogenetic uncoupling of structure and function in human transmodal cortex. doi:10.1101/2021.06.08.447522.
58. Suárez, L. E., Markello, R. D., Betzel, R. F. & Misic, B. Linking Structure and Function in Macroscale Brain Networks. *Trends Cogn. Sci.* **24**, 302–315 (2020).
59. Baum, G. L. *et al.* Development of structure-function coupling in human brain networks during youth. *Proc. Natl. Acad. Sci. U. S. A.* **117**, 771–778 (2020).

60. Paquola, C. *et al.* Microstructural and functional gradients are increasingly dissociated in transmodal cortices. *PLoS Biol.* **17**, e3000284 (2019).
61. Valk, S. L. *et al.* Genetic and phylogenetic uncoupling of structure and function in human transmodal cortex. doi:10.1101/2021.06.08.447522.
62. Van Essen, D. C. *et al.* The WU-Minn Human Connectome Project: an overview. *Neuroimage* **80**, 62–79 (2013).
63. Glasser, M. F. & Van Essen, D. C. Mapping human cortical areas in vivo based on myelin content as revealed by T1- and T2-weighted MRI. *J. Neurosci.* **31**, 11597–11616 (2011).
64. Krienen, F. M. & Sherwood, C. C. Gradients of Connectivity in the Cerebral Cortex. *Trends in cognitive sciences* vol. 21 61–63 (2017).
65. Whelan, C. D. *et al.* Heritability and reliability of automatically segmented human hippocampal formation subregions. *Neuroimage* **128**, 125–137 (2016).
66. Elman, J. A. *et al.* Genetic architecture of hippocampal subfields on standard resolution MRI: How the parts relate to the whole. *Hum. Brain Mapp.* **40**, 1528–1540 (2019).
67. van der Meer, D. *et al.* Brain scans from 21,297 individuals reveal the genetic architecture of hippocampal subfield volumes. *Mol. Psychiatry* **25**, 3053–3065 (2020).
68. Coifman, R. R. & Lafon, S. Diffusion maps. *Applied and Computational Harmonic Analysis* vol. 21 5–30 (2006).
69. Caldairou, B. *et al.* A Surface Patch-Based Segmentation Method for Hippocampal Subfields. *Medical Image Computing and Computer-Assisted Intervention – MICCAI 2016* 379–387 (2016) doi:10.1007/978-3-319-46723-8_44.
70. Glasser, M. F. *et al.* A multi-modal parcellation of human cerebral cortex. *Nature* **536**, 171–178 (2016).
71. Van Essen, D. C., Glasser, M. F., Dierker, D. L., Harwell, J. & Coalson, T. Parcellations and hemispheric asymmetries of human cerebral cortex analyzed on surface-based atlases. *Cereb. Cortex* **22**, 2241–2262 (2012).
72. Wael, R. V. de *et al.* BrainStat: A toolbox for brain-wide statistics and neuroscientific contextualization. doi:10.1101/2022.01.18.476795.
73. Almasy, L. & Blangero, J. Multipoint quantitative-trait linkage analysis in general pedigrees. *Am. J. Hum. Genet.* **62**, 1198–1211 (1998).
74. Whelan, C. D. *et al.* Heritability and reliability of automatically segmented human hippocampal formation subregions. *Neuroimage* **128**, 125–137 (2016).
75. Elman, J. A. *et al.* Genetic architecture of hippocampal subfields on standard resolution MRI: How the parts relate to the whole. *Hum. Brain Mapp.* **40**, 1528–1540 (2019).
76. van der Meer, D. *et al.* Brain scans from 21,297 individuals reveal the genetic architecture of hippocampal subfield volumes. *Mol. Psychiatry* **25**, 3053–3065 (2020).
77. Burt, J. B., Helmer, M., Shinn, M., Anticevic, A. & Murray, J. D. Generative modeling of brain maps with spatial autocorrelation. *Neuroimage* **220**, 117038 (2020).
78. Vos de Wael, R. *et al.* BrainSpace: a toolbox for the analysis of macroscale gradients in neuroimaging and connectomics datasets. *Commun Biol* **3**, 103 (2020).
79. Almasy, L. & Blangero, J. Multipoint quantitative-trait linkage analysis in general pedigrees. *Am. J. Hum. Genet.* **62**, 1198–1211 (1998).
80. Almasy, L., Dyer, T. D. & Blangero, J. Bivariate quantitative trait linkage

analysis: pleiotropy versus co-incident linkages. *Genet. Epidemiol.* **14**, 953–958 (1997).
81. DeKraker, J., Köhler, S. & Khan, A. R. Surface-based hippocampal subfield segmentation. *Trends Neurosci.* **44**, 856–863 (2021).
82. Paquola, C. *et al.* Convergence of cortical types and functional motifs in the human mesiotemporal lobe. *Elife* **9**, (2020).
83. Brunec, I. K. *et al.* Multiple Scales of Representation along the Hippocampal Anteroposterior Axis in Humans. *Curr. Biol.* **28**, 2129–2135.e6 (2018).
84. Chase, H. W. *et al.* Evidence for an anterior-posterior differentiation in the human hippocampal formation revealed by meta-analytic parcellation of fMRI coordinate maps: focus on the subiculum. *Neuroimage* **113**, 44–60 (2015).
85. Poppenk, J., Evensmoen, H. R., Moscovitch, M. & Nadel, L. Long-axis specialization of the human hippocampus. *Trends Cogn. Sci.* **17**, 230–240 (2013).
86. Henriksen, E. J. *et al.* Spatial representation along the proximodistal axis of CA1. *Neuron* **68**, 127–137 (2010).
87. Vogel, J. W. *et al.* A molecular gradient along the longitudinal axis of the human hippocampus informs large-scale behavioral systems. doi:10.1101/587071.
88. Whelan, C. D. *et al.* Heritability and reliability of automatically segmented human hippocampal formation subregions. *Neuroimage* **128**, 125–137 (2016).
89. Elman, J. A. *et al.* Genetic architecture of hippocampal subfields on standard resolution MRI: How the parts relate to the whole. *Hum. Brain Mapp.* **40**, 1528–1540 (2019).
90. van der Meer, D. *et al.* Brain scans from 21,297 individuals reveal the genetic architecture of hippocampal subfield volumes. *Mol. Psychiatry* **25**, 3053–3065 (2020).
91. Zhao, B. *et al.* Heritability of Regional Brain Volumes in Large-Scale Neuroimaging and Genetic Studies. *Cereb. Cortex* **29**, 2904–2914 (2019).
92. Hibar, D. P. *et al.* Novel genetic loci associated with hippocampal volume. *Nat. Commun.* **8**, 13624 (2017).
93. Hibar, D. P. *et al.* Common genetic variants influence human subcortical brain structures. *Nature* **520**, 224–229 (2015).
94. Stein, J. L. *et al.* Identification of common variants associated with human hippocampal and intracranial volumes. *Nat. Genet.* **44**, 552–561 (2012).
95. Maller, J. J. *et al.* Hippocampal volumetrics in treatment-resistant depression and schizophrenia: the devil's in de-tail. *Hippocampus* **22**, 9–16 (2012).
96. Warland, A., Kendall, K. M., Rees, E., Kirov, G. & Caseras, X. Schizophrenia-associated genomic copy number variants and subcortical brain volumes in the UK Biobank. *Mol. Psychiatry* **25**, 854–862 (2020).
97. Valk, S. L. *et al.* Genetic and phylogenetic uncoupling of structure and function in human transmodal cortex. doi:10.1101/2021.06.08.447522.
98. Arnatkeviciute, A. *et al.* Genetic influences on hub connectivity of the human connectome. *Nat. Commun.* **12**, 4237 (2021).
99. Haak, K. V. & Beckmann, C. F. Plasticity versus stability across the human cortical visual connectome. *Nat. Commun.* **10**, 3174 (2019).
100. Glasser, M. F. *et al.* A multi-modal parcellation of human cerebral cortex. *Nature* **536**, 171–178 (2016).
101. Assem, M., Glasser, M. F., Van Essen, D. C. & Duncan, J. A Domain-General Cognitive Core Defined in Multimodally Parcellated Human Cortex. *Cereb. Cortex* **30**,

4361–4380 (2020).
102. Ganzetti, M., Wenderoth, N. & Mantini, D. Whole brain myelin mapping using T1- and T2-weighted MR imaging data. *Front. Hum. Neurosci.* **8**, 671 (2014).
103. Glasser, M. F. & Van Essen, D. C. Mapping Human Cortical Areas In Vivo Based on Myelin Content as Revealed by T1- and T2-Weighted MRI. *Journal of Neuroscience* vol. 31 11597–11616 (2011).
104. Burt, J. B. *et al.* Hierarchy of transcriptomic specialization across human cortex captured by structural neuroimaging topography. *Nature Neuroscience* vol. 21 1251–1259 (2018).
105. Lorio, S. *et al.* Neurobiological origin of spurious brain morphological changes: A quantitative MRI study. *Hum. Brain Mapp.* **37**, 1801–1815 (2016).
106. Stüber, C. *et al.* Myelin and iron concentration in the human brain: A quantitative study of MRI contrast. *NeuroImage* vol. 93 95–106 (2014).
107. Paquola, C. *et al.* Microstructural and functional gradients are increasingly dissociated in transmodal cortices. *PLoS Biol.* **17**, e3000284 (2019).
108. Vogt, C. & Vogt, O. Die Grundlagen und die Teildisziplinen der mikroskopischen Anatomie des Zentralnervensystems. *Nervensystem* 448–477 (1928) doi:10.1007/978-3-642-66443-4_8.
109. Vos de Wael, R. *et al.* Anatomical and microstructural determinants of hippocampal subfield functional connectome embedding. *Proc. Natl. Acad. Sci. U. S. A.* **115**, 10154–10159 (2018).
110. Bernhardt, B. C. *et al.* Preferential susceptibility of limbic cortices to microstructural damage in temporal lobe epilepsy: A quantitative T1 mapping study. *NeuroImage* vol. 182 294–303 (2018).
111. Kim, E. J., Pellman, B. & Kim, J. J. Stress effects on the hippocampus: a critical review. *Learning & Memory* vol. 22 411–416 (2015).
112. McEwen, B. S. Stress and hippocampal plasticity. *Annu. Rev. Neurosci.* **22**, 105–122 (1999).
113. Gratton, C. *et al.* Functional Brain Networks Are Dominated by Stable Group and Individual Factors, Not Cognitive or Daily Variation. *Neuron* vol. 98 439–452.e5 (2018).
114. Cooper, C. 'iana, Moon, H. Y. & van Praag, H. On the Run for Hippocampal Plasticity. *Cold Spring Harb. Perspect. Med.* **8**, (2018).
115. Barth, C. *et al.* In-vivo Dynamics of the Human Hippocampus across the Menstrual Cycle. *Sci. Rep.* **6**, 32833 (2016).
116. Zsido, R. G. *et al.* Longitudinal 7T MRI reveals volumetric changes in subregions of human medial temporal lobe to sex hormone fluctuations. doi:10.1101/2022.05.02.490281.
117. Kim, E. J., Pellman, B. & Kim, J. J. Stress effects on the hippocampus: a critical review. *Learning & Memory* vol. 22 411–416 (2015).
118. McEwen, B. S. Stress and hippocampal plasticity. *Annu. Rev. Neurosci.* **22**, 105–122 (1999).
119. Alexander-Bloch, A., Raznahan, A., Bullmore, E. & Giedd, J. The convergence of maturational change and structural covariance in human cortical networks. *J. Neurosci.* **33**, 2889–2899 (2013).
120. Valk, S. L. *et al.* Shaping brain structure: Genetic and phylogenetic axes of macroscale organization of cortical thickness. *Sci Adv* **6**, (2020).

121. Paquola, C. *et al.* Microstructural and functional gradients are increasingly dissociated in transmodal cortices. *PLoS Biol.* **17**, e3000284 (2019).
122. Burt, J. B. *et al.* Hierarchy of transcriptomic specialization across human cortex captured by structural neuroimaging topography. *Nature Neuroscience* vol. 21 1251–1259 (2018).
123. Cahalane, D. J., Charvet, C. J. & Finlay, B. L. Modeling local and cross-species neuron number variations in the cerebral cortex as arising from a common mechanism. *Proc. Natl. Acad. Sci. U. S. A.* **111**, 17642–17647 (2014).
124. Fornito, A., Arnatkevičiūtė, A. & Fulcher, B. D. Bridging the Gap between Connectome and Transcriptome. *Trends Cogn. Sci.* **23**, 34–50 (2019).
125. Alexander-Bloch, A. F. *et al.* Human Cortical Thickness Organized into Genetically-determined Communities across Spatial Resolutions. *Cereb. Cortex* **29**, 106–118 (2019).
126. Chen, C.-H. *et al.* Genetic topography of brain morphology. *Proc. Natl. Acad. Sci. U. S. A.* **110**, 17089–17094 (2013).
127. Vogel, J. W. *et al.* A molecular gradient along the longitudinal axis of the human hippocampus informs large-scale behavioral systems. *Nature Communications* vol. 11 (2020).
128. Taupin, P. *The Hippocampus: Neurotransmission and Plasticity in the Nervous System*. (Nova Publishers, 2007).
129. Jabès, A., Lavenex, P. B., Amaral, D. G. & Lavenex, P. Postnatal development of the hippocampal formation: a stereological study in macaque monkeys. *J. Comp. Neurol.* **519**, 1051–1070 (2011).
130. Insausti, R., Cebada-Sánchez, S. & Marcos, P. Postnatal Development of the Human Hippocampal Formation. *Advances in Anatomy, Embryology and Cell Biology* (2010) doi:10.1007/978-3-642-03661-3.
131. van Praag, H., Kempermann, G. & Gage, F. H. Neural consequences of enviromental enrichment. *Nature Reviews Neuroscience* vol. 1 191–198 (2000).
132. Zocher, S., Overall, R. W., Lesche, M., Dahl, A. & Kempermann, G. Environmental enrichment preserves a young DNA methylation landscape in the aged mouse hippocampus. *Nature Communications* vol. 12 (2021).
133. Smith, K. E. & Pollak, S. D. Early life stress and development: potential mechanisms for adverse outcomes. *J. Neurodev. Disord.* **12**, 34 (2020).
134. Hanson, J. L. *et al.* Behavioral problems after early life stress: contributions of the hippocampus and amygdala. *Biol. Psychiatry* **77**, 314–323 (2015).
135. Teicher, M. H. *et al.* Differential effects of childhood neglect and abuse during sensitive exposure periods on male and female hippocampus. *Neuroimage* **169**, 443–452 (2018).
136. Gorka, A. X., Hanson, J. L., Radtke, S. R. & Hariri, A. R. Reduced hippocampal and medial prefrontal gray matter mediate the association between reported childhood maltreatment and trait anxiety in adulthood and predict sensitivity to future life stress. *Biol. Mood Anxiety Disord.* **4**, 12 (2014).
137. Chao, L. L., Tosun, D., Woodward, S. H., Kaufer, D. & Neylan, T. C. Preliminary Evidence of Increased Hippocampal Myelin Content in Veterans with Posttraumatic Stress Disorder. *Front. Behav. Neurosci.* **9**, 333 (2015).
138. Baum, G. L. *et al.* Development of structure-function coupling in human brain

networks during youth. *Proc. Natl. Acad. Sci. U. S. A.* **117**, 771–778 (2020).
139. Buzsáki, G. & Tingley, D. Space and Time: The Hippocampus as a Sequence Generator. *Trends Cogn. Sci.* **22**, 853–869 (2018).
140. Wagner, A. D., Shannon, B. J., Kahn, I. & Buckner, R. L. Parietal lobe contributions to episodic memory retrieval. *Trends Cogn. Sci.* **9**, 445–453 (2005).
141. Fanselow, M. S. & Dong, H.-W. Are the dorsal and ventral hippocampus functionally distinct structures? *Neuron* **65**, 7–19 (2010).
142. Save, E., Poucet, B., Foreman, N. & Buhot, M.-C. Object exploration and reactions to spatial and nonspatial changes in hooded rats following damage to parietal cortex or hippocampal formation. *Behavioral Neuroscience* vol. 106 447–456 (1992).
143. Corbetta, M. & Shulman, G. L. Spatial neglect and attention networks. *Annu. Rev. Neurosci.* **34**, 569–599 (2011).
144. Van Essen, D. C. *et al.* The WU-Minn Human Connectome Project: an overview. *Neuroimage* **80**, 62–79 (2013).
145. Caldairou, B. *et al.* A Surface Patch-Based Segmentation Method for Hippocampal Subfields. *Medical Image Computing and Computer-Assisted Intervention – MICCAI 2016* 379–387 (2016) doi:10.1007/978-3-319-46723-8_44.
146. Glasser, M. F. *et al.* The minimal preprocessing pipelines for the Human Connectome Project. *Neuroimage* **80**, 105–124 (2013).
147. Patenaude, B., Smith, S. M., Kennedy, D. N. & Jenkinson, M. A Bayesian model of shape and appearance for subcortical brain segmentation. *NeuroImage* vol. 56 907–922 (2011).
148. Dale, A. M., Fischl, B. & Sereno, M. I. Cortical surface-based analysis. I. Segmentation and surface reconstruction. *Neuroimage* **9**, 179–194 (1999).
149. Fischl, B., Sereno, M. I. & Dale, A. M. Cortical Surface-Based Analysis. *NeuroImage* vol. 9 195–207 (1999).
150. Fischl, B., Sereno, M. I., Tootell, R. B. H. & Dale, A. M. High-resolution intersubject averaging and a coordinate system for the cortical surface. *Human Brain Mapping* vol. 8 272–284 (1999).
151. Greve, D. N. & Fischl, B. Accurate and robust brain image alignment using boundary-based registration. *Neuroimage* **48**, 63–72 (2009).
152. Salimi-Khorshidi, G. *et al.* Automatic denoising of functional MRI data: combining independent component analysis and hierarchical fusion of classifiers. *Neuroimage* **90**, 449–468 (2014).
153. Caldairou, B. *et al.* A Surface Patch-Based Segmentation Method for Hippocampal Subfields. *Medical Image Computing and Computer-Assisted Intervention – MICCAI 2016* 379–387 (2016) doi:10.1007/978-3-319-46723-8_44.
154. Kulaga-Yoskovitz, J. *et al.* Multi-contrast submillimetric 3 Tesla hippocampal subfield segmentation protocol and dataset. *Sci Data* **2**, 150059 (2015).
155. Styner, M. *et al.* Framework for the Statistical Shape Analysis of Brain Structures using SPHARM-PDM. *Insight J.* 242–250 (2006).
156. Kim, H. *et al.* Multivariate hippocampal subfield analysis of local MRI intensity and volume: application to temporal lobe epilepsy. *Med. Image Comput. Comput. Assist. Interv.* **17**, 170–178 (2014).
157. Marcus, D. S. *et al.* Informatics and data mining tools and strategies for the human connectome project. *Front. Neuroinform.* **5**, 4 (2011).

158. Kochunov, P. *et al.* Homogenizing Estimates of Heritability Among SOLAR-Eclipse, OpenMx, APACE, and FPHI Software Packages in Neuroimaging Data. *Front. Neuroinform.* **13**, 16 (2019).
159. Glahn, D. C. *et al.* Genetic control over the resting brain. *Proc. Natl. Acad. Sci. U. S. A.* **107**, 1223–1228 (2010).
160. Vos de Wael, R. *et al.* Anatomical and microstructural determinants of hippocampal subfield functional connectome embedding. *Proc. Natl. Acad. Sci. U. S. A.* **115**, 10154–10159 (2018).
161. Vos de Wael, R. *et al.* BrainSpace: a toolbox for the analysis of macroscale gradients in neuroimaging and connectomics datasets. *Commun Biol* **3**, 103 (2020).
162. Valk, S. L. *et al.* Genetic and phylogenetic uncoupling of structure and function in human transmodal cortex. *Nat. Commun.* **13**, 2341 (2022).
163. Vázquez-Rodríguez, B. *et al.* Gradients of structure-function tethering across neocortex. doi:10.1101/561985.
164. Yeo, B. T. T. *et al.* The organization of the human cerebral cortex estimated by intrinsic functional connectivity. *Journal of Neurophysiology* vol. 106 1125–1165 (2011).
165. Burt, J. B., Helmer, M., Shinn, M., Anticevic, A. & Murray, J. D. Generative modeling of brain maps with spatial autocorrelation. *Neuroimage* **220**, 117038 (2020).

Supplementary Materials

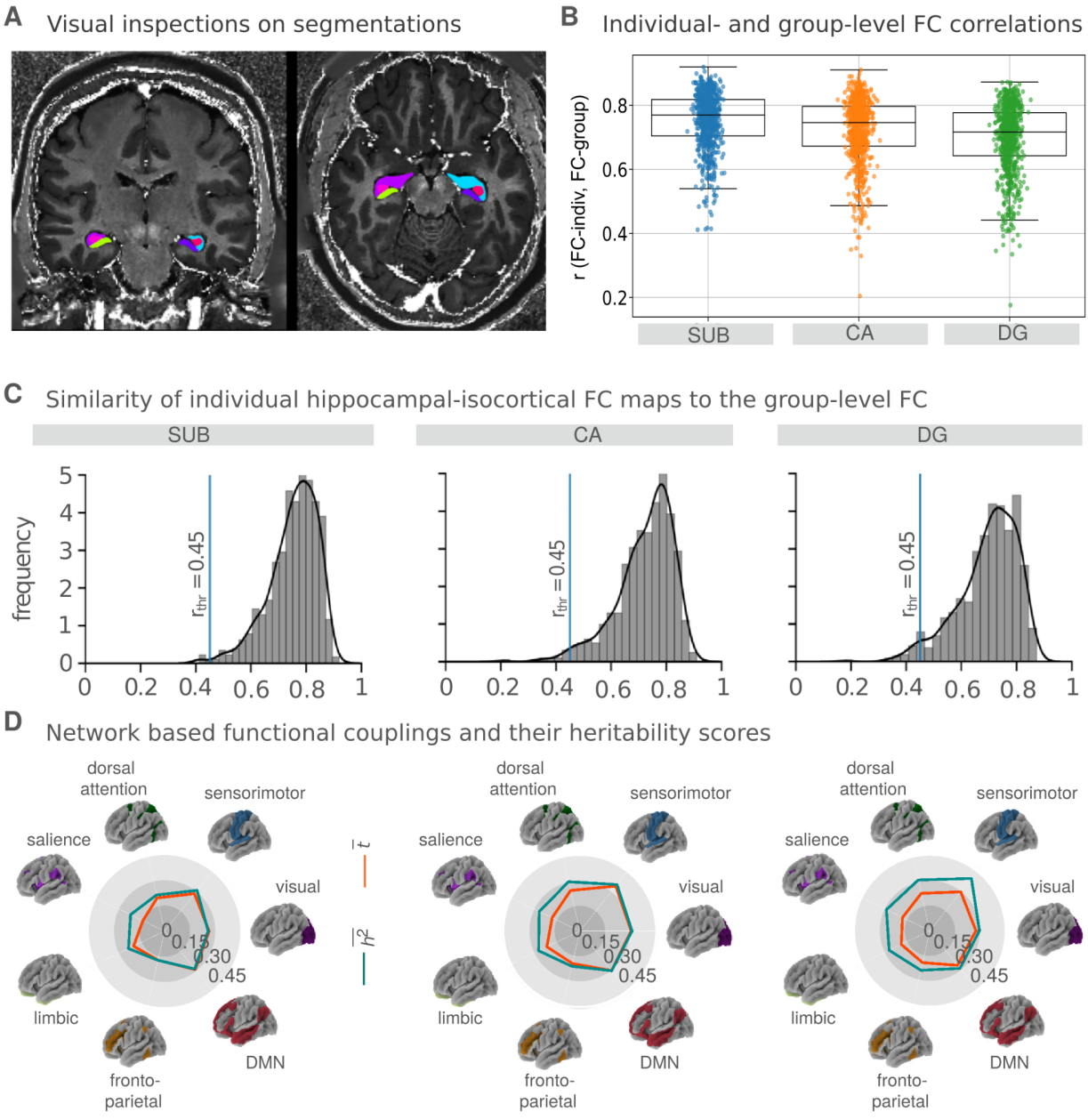

Supplementary Fig. S1. Quality assessment for the individual hippocampal-isocortical functional connectivity (FC) profiles and network-level representations of the group-level hippocampal-isocortical FC. A. A randomly chosen participant from HCP S900 data release with the hippocampal subfield segmentations overlaid on coronal and transverse planes on T1 image. All SurfPatch segmentations underwent a visual inspection for a quality assurance. **B.** Individual level functional connectivity (FC) matrices correlated (Pearson's r) with the group level FC for n = 740 participants (y-

axis) for each subfield (x-axis). Group level FC was assessed by averaging subfield-to-cortex FC matrices for SUB (left and right hemisphere; L & R), for CA (L & R), and for DG (L & R). The mean correlation and 2.5 standard deviation of the mean was found to be 0.75 ± 0.21 for SUB, 0.72 ± 0.25 for CA and 0.70 ± 0.28 for DG. **C.** FC similarity of n = 740 participants to the group-level FC quantified by means of Pearson's correlations (r). Threshold r-value (r_{thr} = 0.45) was assessed by computing the 2.5 standard deviation distance away from the mean r-values. Participants with a lower degree of similarity (r_{thr} < 0.45, n = 31) were excluded prior to the functional connectome gradient analysis. **D.** Hippocampal-isocortical FC strength (t-values) and its heritability (h^2scores) distributed into seven networks [1]. The t-values and h^2scores were averaged ($\bar{t}$ and $\overline{h^2}$ red and blue, respectively) within each single network and demonstrated with a spyder plot.

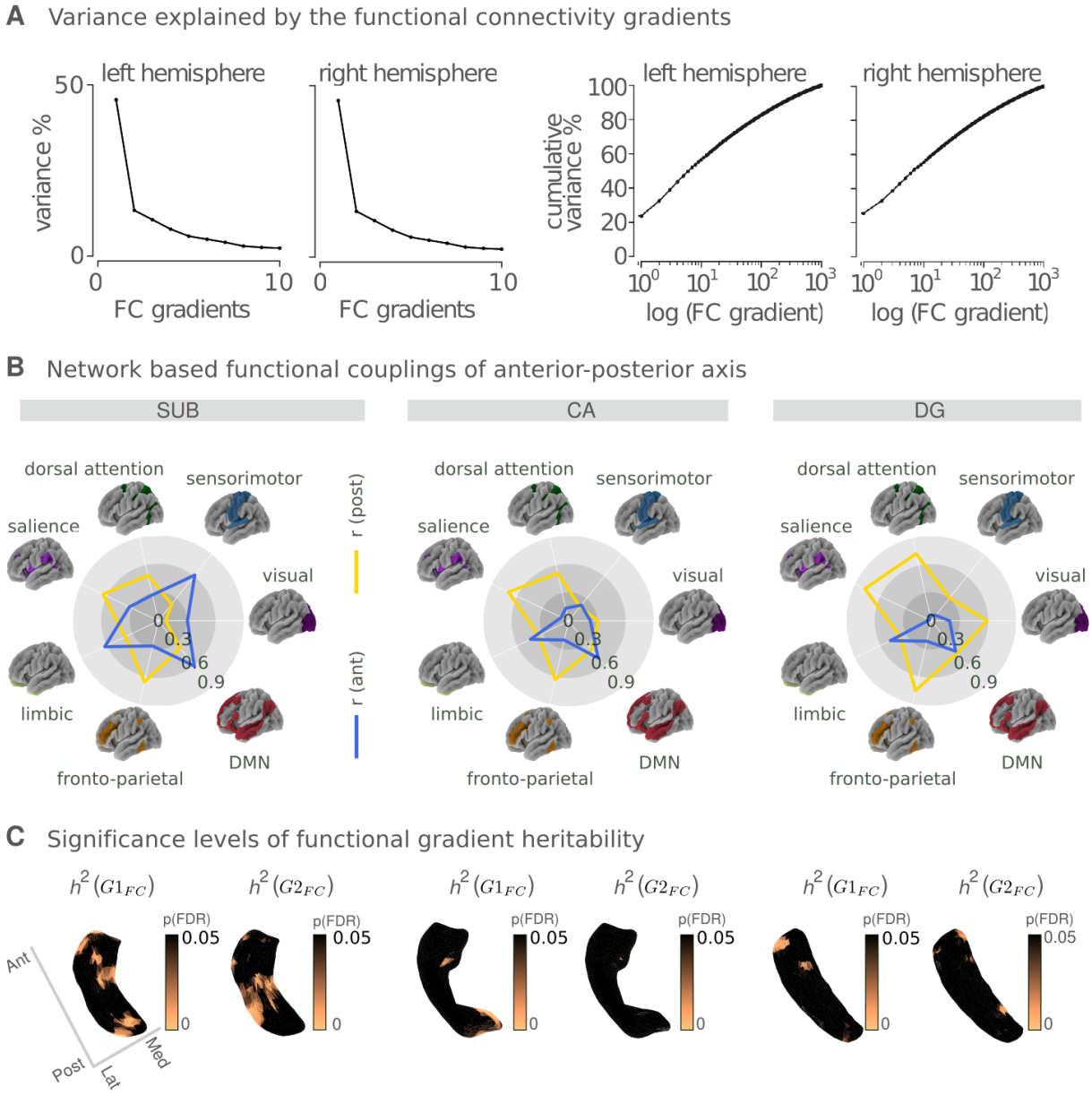

Supplementary Fig. S2. Connectivity gradients of hippocampal-isocortical functional connectivity (FC) and their heritability. A. Variance explained by the first 10 FC gradients (left) and first 1000 FC gradients (right) for both hemispheres. Left: The first 10 FC gradients were used throughout the manuscript. Right: The first 1000 FC gradients were obtained as a control analysis. Cumulative variance explained by the first three gradients was 38.5% for the left hemisphere and 38.9% for the right hemisphere. **B.** FC from anterior (r-values, blue) and posterior (r-values, yellow) subfield portions revealed by the $G1_{FC}$ were distributed into seven large-scale functional networks [1]. **C.** Significance levels of gradient map heritability ($h^2(G1_{FC})$ and $h^2(G2_{FC})$) reported by p(FDR).

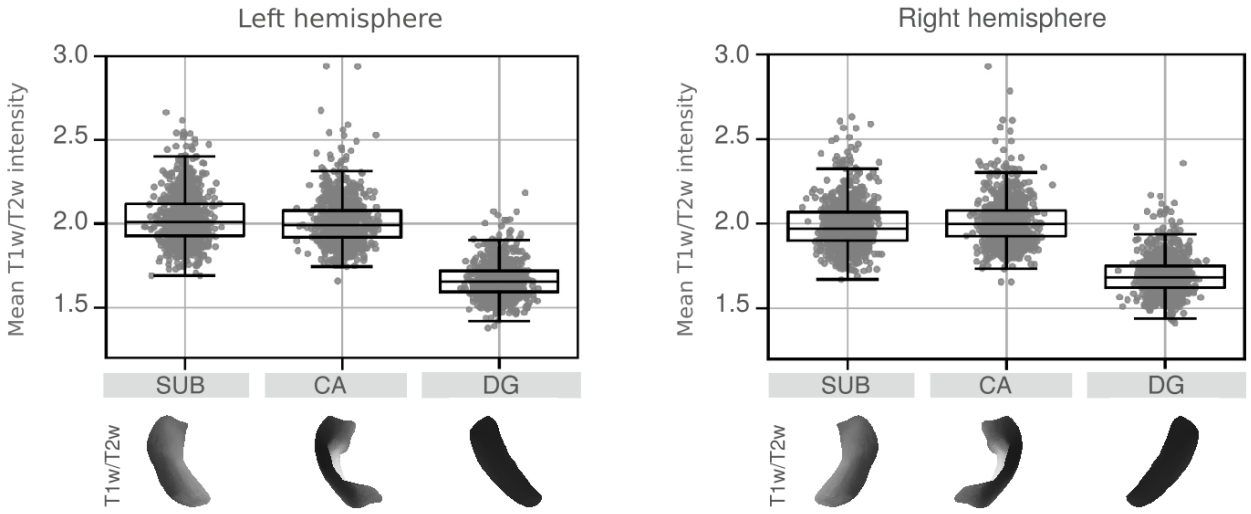

Supplementary Fig. S3. Quality assessment on individual (n = 709) T1w/T2w intensity maps for left and right hemispheres. Mean T1w/T2w intensity map distributions for each subject (n = 709, x-axis) and each subfield (SUB, CA, DG, y-axis) are depicted for left and right hemispheres, separately. For the left hemisphere, mean and standard deviations of T1w/T2w maps were 2.02 $\pm$ 0.41 for SUB, 2.01 $\pm$ 0.78 for CA, and 1.66 $\pm$ 0.22 for DG. For the right hemisphere, mean and standard deviations of T1w/T2w maps were 1.99 $\pm$ 0.43 for SUB, 2.01 $\pm$ 0.68 for CA, and 1.69 $\pm$ 0.23 for DG.

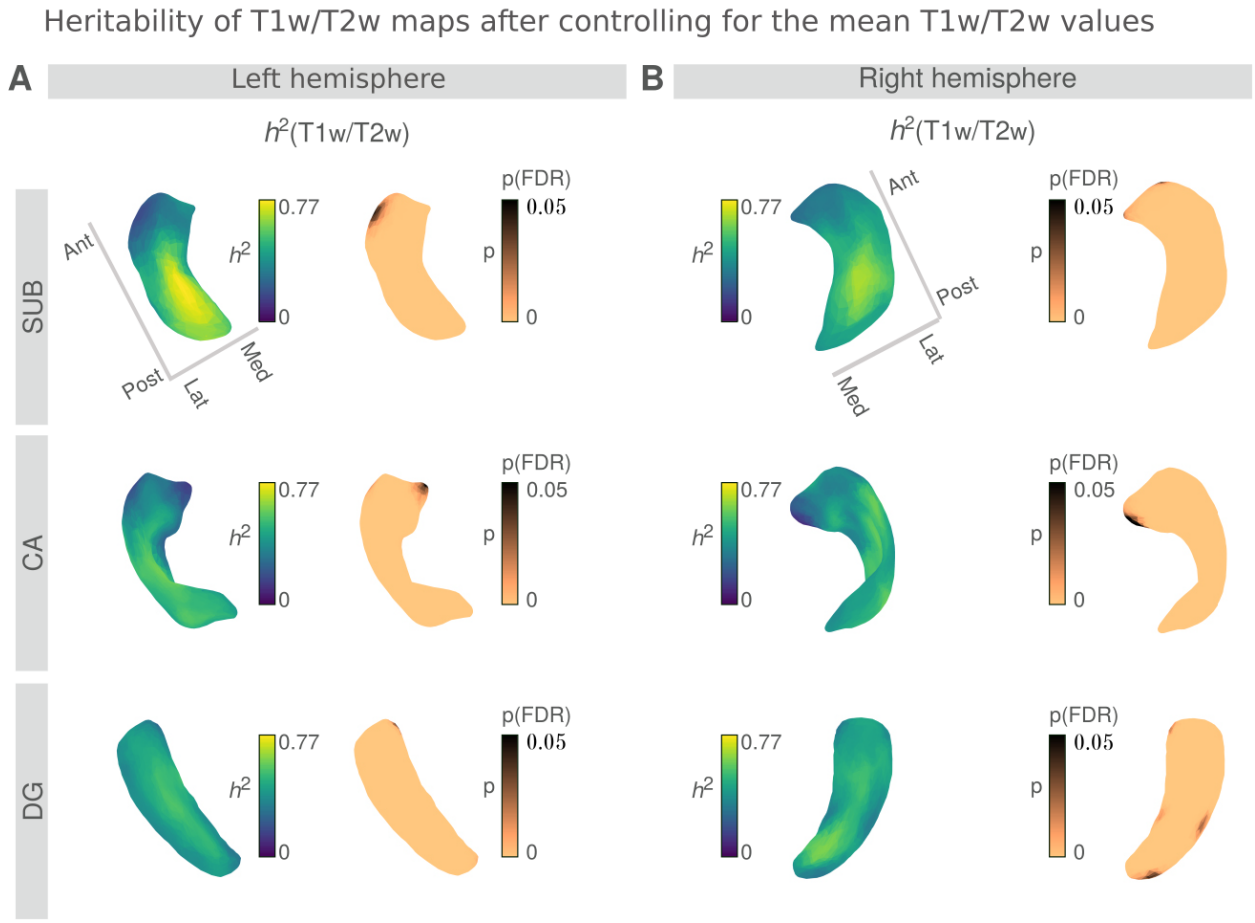

Supplementary Fig. S4. Heritability of the T1w/T2w intensity maps (h^2(T1w/T2w)) by controlling for the mean T1w/T2w intensities for each subfield (SUB, CA, DG) and hemisphere (left and right). **A.** h^2(T1w/T2w) patterns and their FDR-corrected significance levels (p(FDR)) did not change after controlling for the mean T1w/T2w intensities for the left hemisphere (copper color denotes pFDR < 0.05, black pFDR > 0.05). **B.** Similar results were observed for the right hemisphere.

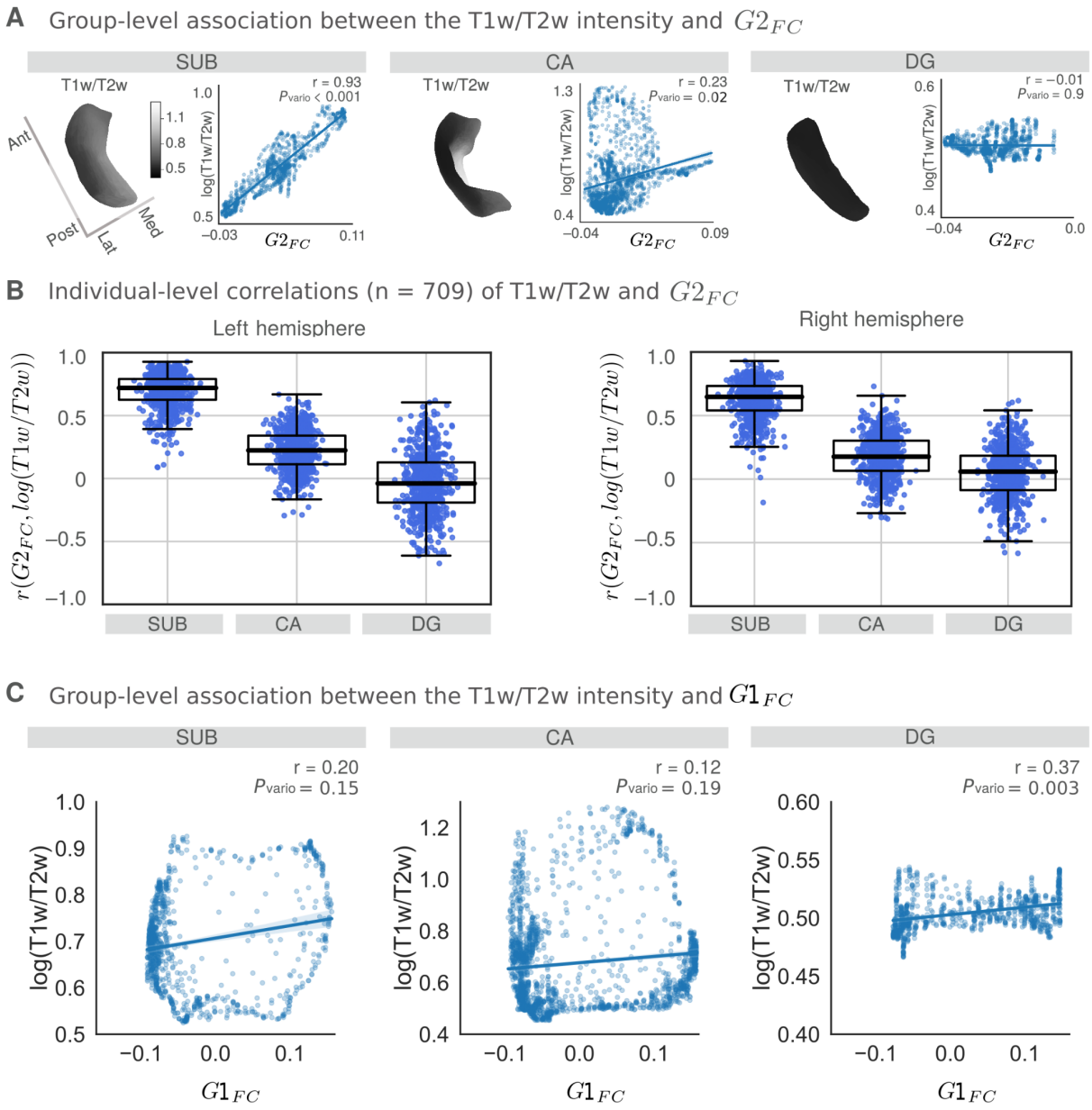

Supplementary Fig. S5. Spatial association between T1w/T2w intensity maps and the medial-lateral organisational axis represented by $G2_{FC}$. A. Group-level association between the mean T1w/T2w profiles and the $G2_{FC}$ for each subfield. The T1w/T2w profiles of subfields correlate strongly with the $G2_{FC}$ for SUB (r = 0.93 and p_{vario} < 0.001), however, not for the CA (r = 0.23 and p_{vario} = 0.02) or DG (r = -0.01 and p_{vario} = 0.9). **B.** Individual-level correlations (n = 709) between $G2_{FC}$ maps and T1w/T2w intensity maps for each subfield (SUB, CA, DG) and hemisphere (left and right). For the left hemisphere, individual correlations (r($G2_{FC}$, log(T1w/T2w)) were significantly positive for the SUB (median $\overline{r}$ = 0.72, p < 0.005, one-tailed Wilcoxon signed-rank test) and CA ($\overline{r}$ = 0.22, p < 0.005), however not for DG ($\overline{r}$ = -0.04, p < 0.1). Similar results were observed along the subfields in the right hemisphere (SUB: $\overline{r}$ = 0.65, p < 0.005, CA: $\overline{r}$ = 0.18, p < 0.005, DG: $\overline{r}$ = 0.06, p < 0.1). **C.** Group-level association between the mean T1w/T2w profiles and the $G1_{FC}$ for each subfield. The T1w/T2w profiles of subfields do not correlate well with the $G1_{FC}$ for SUB (r = 0.20 and p_{vario} = 0.15), CA (r = 0.12 and p_{vario} = 0.19) or DG (r = 0.39 and p_{vario} = 0.003).

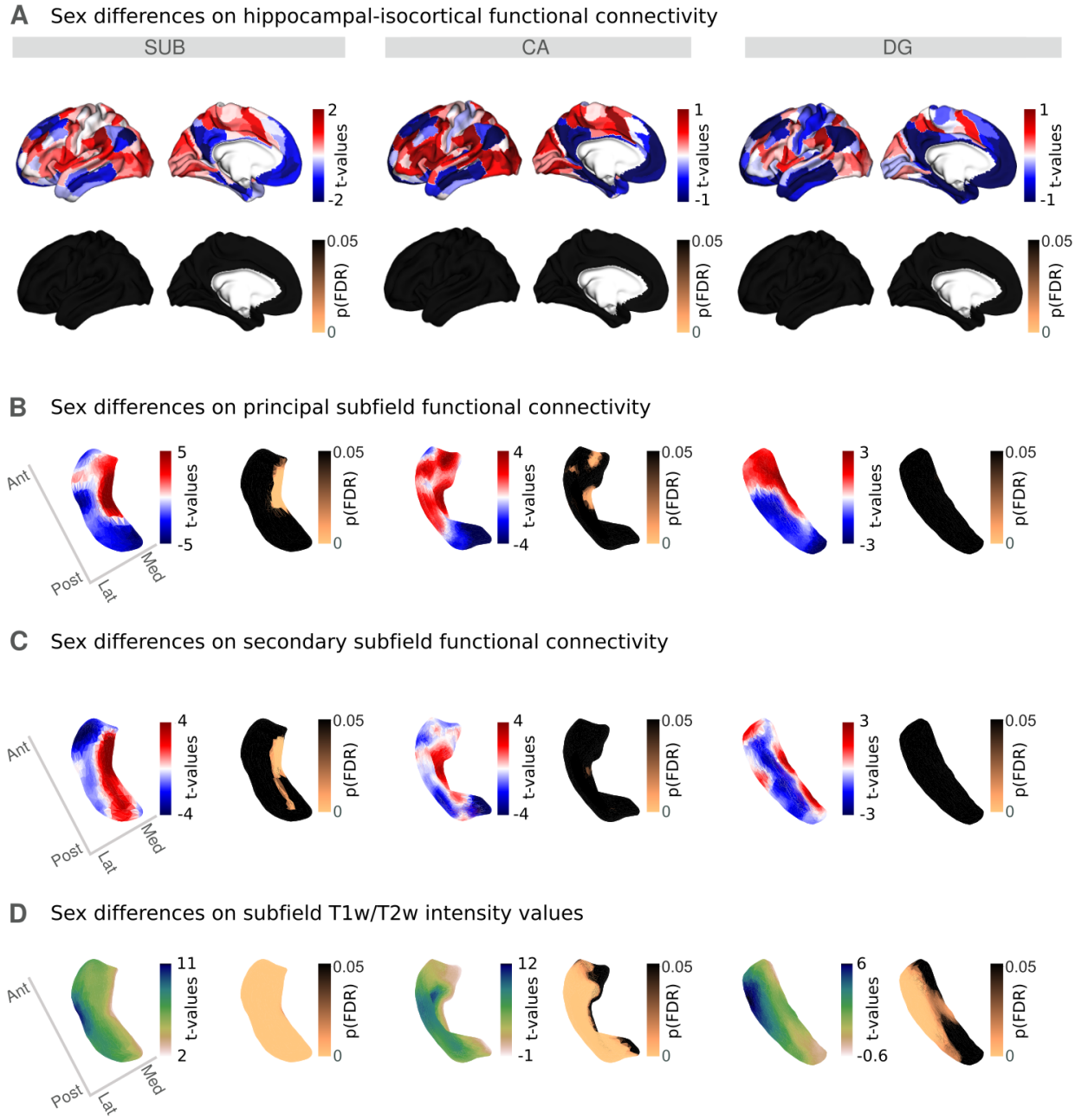

Supplementary Fig. S6. Sex differences illustrated for subfield-isocortical functional connectivity (FC), connectome gradients, and T1w/T2w measures. For each measure of interest, participants' sex is assigned as a fixed effect (+1 for males and -1 for females) and a linear model is run by contrasting this fixed effect. T-values represent the degree of sex effects and FDR corrected p-values (p(FDR)) depict their significance levels. **A.** There is no significant effect of sex on the subfield-isocortical FC. **B.** Sex differences on principal functional connectivity gradient $G1_{\square\square}$ was observed to be significant on antero-medial portions of SUB and CA, however, not for DG. **C.** Sex difference on secondary functional connectivity gradient $G2_{\square\square}$ was observed to be significant on antero-medial portions of SUB, extending further to the posterior portions, however, not significant for CA and DG. **D.** Sex differences on T1w/T2w intensity maps had significant effects on whole SUB, and large portions of CA and DG except for their anterior and posterior portions.

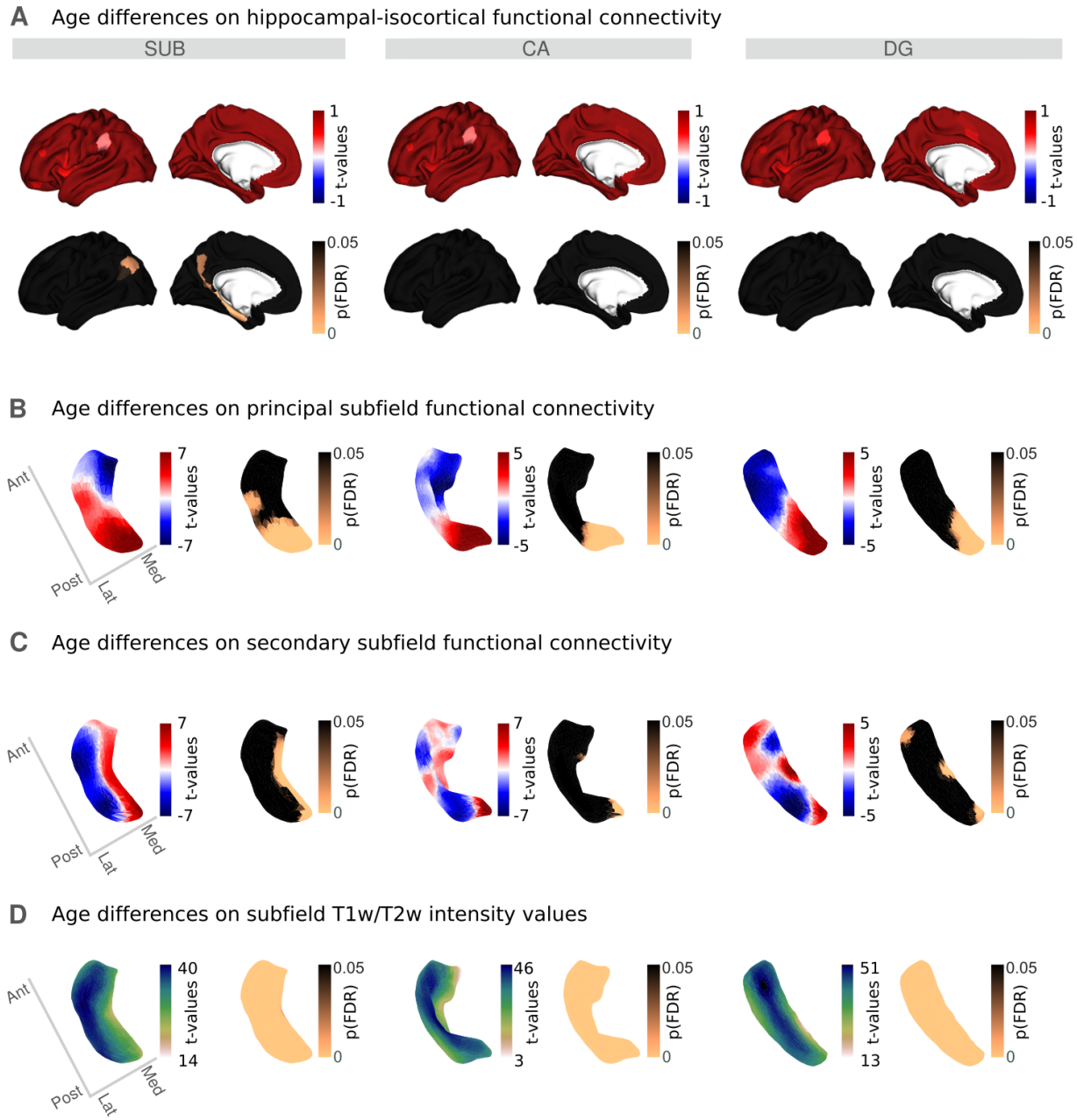

Supplementary Fig. S7. Age differences illustrated for subfield-isocortical functional connectivity (FC), connectome gradients, and T1w/T2w measures. For each measure of interest, participants' age is assigned as a fixed effect and a linear model is run by contrasting this fixed effect. T-values represent the degree of age effects and FDR corrected p-values (p(FDR)) depict their significance levels. **A.** Age effect was observed to be significant in hippocampus itself and angular gyrus for the SUB-isocortex FC, however not significant for CA- and DG-isocortex FC. **B.** Age effect on principal functional connectivity gradient $G1_{\square\square}$ was observed to be significant in posterior portions of all subfields SUB, CA and DG. **C.** Age effect on secondary functional connectivity gradient $G2_{\square\square}$ was observed to be significant in medial portions of SUB, small posterior portions of CA and DG. **D.** Age effect on T1w/T2w intensity maps had significant effects on the whole SUB, CA and DG.

We illustrated the sex and age effects on subfield functional and microstructural organisational axes (**Fig. S6, S7**). For the subfield-isocortical FC, there was no significant sex effect (**Fig. S6A**). For the subfield $G1_{FC}$, we observed significant sex effects on antero-medial portions of SUB and CA, however, not for DG (**Fig. S6B**). For the $G2_{FC}$, there were significant sex effects on antero-medial portions of SUB, extending further to the posterior portions, however, not significant for CA and DG (**Fig. S6C**). Sex differences became significant on T1w/T2w intensity maps throughout whole SUB, and large portions of CA and DG except for their anterior and posterior portions (**Fig. S6D**). On the other hand, the age effect was observed to be significant in hippocampus itself and angular gyrus for the SUB-isocortex FC, however not significant for CA- and DG-isocortex FC (**Fig. S7A**). For the subfield $G1_{FC}$, we observed significant age effects in posterior portions of all subfields SUB, CA and DG (**Fig. S7B**). For the $G2_{FC}$, there were significant sex effects in medial portions of SUB, small posterior portions of CA and DG (**Fig. S7C**). Age differences became significant on T1w/T2w intensity maps for the whole SUB, CA and DG (**Fig. S7D**).

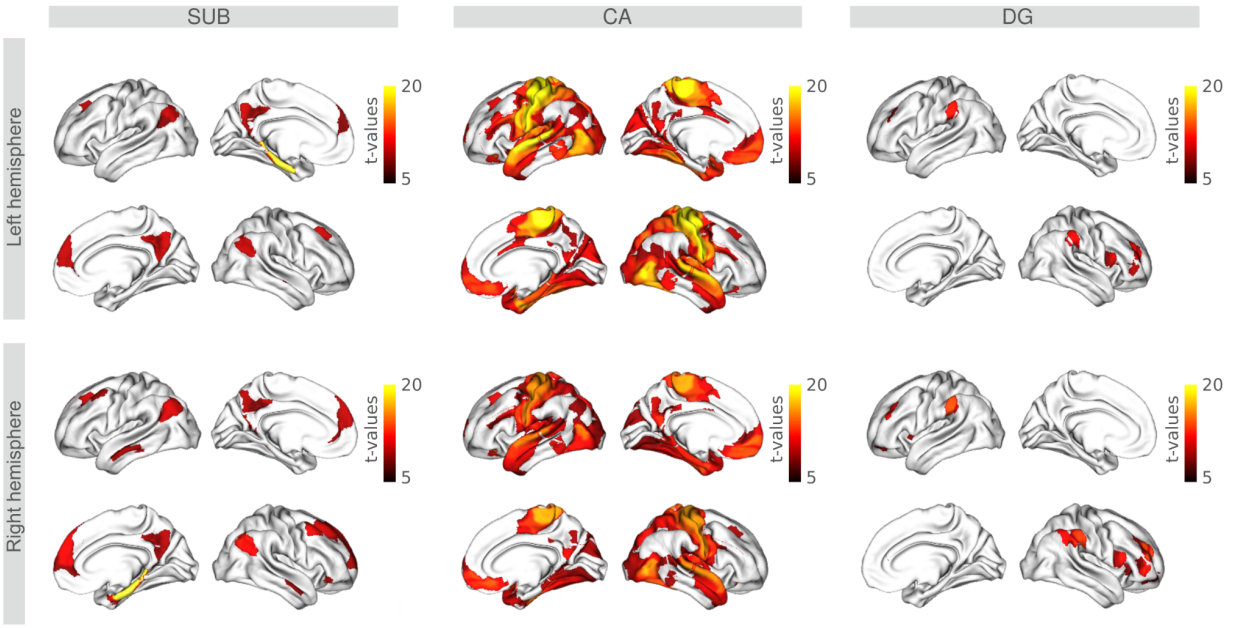

Supplementary Fig. S8. A single-subfield specific functional connectivity (FC) to the isocortex after contrasting with the FC of the other two subfields. SUB-isocortical FC is higher in default mode network, CA-isocortical FC is stronger in somatomor and limbic areas, whereas DG-isocortex did not demonstrate particularly high or specific FC patterns.

Supplementary Table T1. Spatial similarity of subiculum (SUB) organisational axes computed in a pairwise fashion. Similarity is computed by Pearson's r and its significance reported by the p_{vario}; the p-value after spatial autocorrelation correction [165]. The autocorrelations were assessed by using the SUB vertex coordinate and edge information as well as their n = 1000 simulated surrogate coordinates.

SUB	$G1_{FC}$	$G2_{FC}$	G1 (h^2)	G2 (h^2)	$G1_{SiC}$	$G2_{SiC}$	$G1_{GEN}$	$G2_{GEN}$	T1w/T2w	Coupling
$G1_{FC}$			**r = 0.89, p_{vario} < 0.001**	r = 0.17, p_{vario} = 0.18	**r = 0.88, p_{vario} < 0.001**	**r = 0.75, p_{vario}< 0.001**	**r = 0.67, p_{vario} < 0.001**	r = -0.01, p_{vario} = 0.89	r = 0.20, p_{vario} = 0.15	0.34 r = 0.34, p_{vario}= 0.01
$G2_{FC}$			r = 0.33, p_{vario} = 0.02	**r = 0.70, p_{vario} < 0.001**	r = 0.45, p_{vario} = 0.003	r = 0.36, p_{vario}= 0.007	r = 0.29, p_{vario} = 0.03	r = 0.02, p_{vario} = 0.89	**r =0.93, p_{vario} < 0.001**	**r = -0.59, p_{vario}< 0.001**
G1 (h^2)					**r = 0.78, p_{vario} < 0.001**	**r = 0.64,p_{vario} < 0.001**	**r = 0.61, p_{vario} < 0.001**	r = -0.02, p_{vario} = 0.86	r = 0.24, p_{vario} = 0.07	r = 0.22, p_{vario}= 0.09
G2 (h^2)					r = 0.24, p_{vario} = 0.09	r = 0.22, p_{vario}= 0.01	r = 0.30, p_{vario} = 0.05	r = 0.27, p_{vario} = 0.04	**r = 0.69, p_{vario} < 0.001**	r = -0.38, p_{vario}= 0.01
$G1_{SiC}$							**r = 0.76, p_{vario} < 0.001**	r = -0.23, p_{vario} = 0.07	r = 0.38, p_{vario} = 0.01	r = 0.24, p_{vario}= 0.10
$G2_{SiC}$							**r = 0.81, p_{vario} < 0.001**	r = 0.01, p_{vario} = 0.91	r = 0.37, p_{vario} = 0.01	r = 0.23, p_{vario}= 0.10
$G1_{GEN}$									r = 0.32, p_{vario} = 0.02	r = 0.30, p_{vario}= 0.04
$G2_{GEN}$									r = 0.06, p_{vario} = 0.06	r = -0.07, p_{vario}= 0.05
T1w/T2w										**r = -0.59,p_{vario} < 0.001**

Supplementary Table T2. Spatial similarity of cornu ammonis (CA) organisational axes computed in a pairwise fashion. Similarity is computed by Pearson's r and its significance reported by the p_{vario}; the p-value after spatial autocorrelation correction [77]. The autocorrelations were assessed by using the CA vertex coordinate and edge information as well as their n = 1000 simulated surrogate coordinates.

CA	$G1_{FC}$	$G2_{FC}$	G1 (h^2)	G2 (h^2)	$G1_{SiC}$	$G2_{SiC}$	$G1_{GEN}$	$G2_{GEN}$	T1w/T2w	Coupling
$G1_{FC}$			**r = 0.83,** p_{vario}< **0.001**	r =0.04, p_{vario}= 0.06	**r =0.86,** p_{vario}< **0.001**	r = 0.13, p_{vario}= 0.13	**r = 0.41,** p_{vario}< **0.001**	**r = -0.52,** p_{vario}< **0.001**	r = 0.12, p_{vario}= 0.19	**r = 0.72,** p_{vario}< **0.001**
$G2_{FC}$			r = 0.13, p_{vario}= 0.16	**r = 0.74,** p_{vario}< **0.001**	r = 0.28, p_{vario}= 0.007	r =0.22, p_{vario}= 0.02	r = 0.32, p_{vario}= 0.001	r = -0.02, p_{vario}= 0.75	r = 0.23, p_{vario}= 0.02	r = 0.10, p_{vario}= 0.05
G1 (h^2)					**r = 0.74,** p_{vario}< **0.001**	r = 0.12, p_{vario}= 0.19	r = 0.16, p_{vario}= 0.09	**r = -0.49,** p_{vario}< **0.001**	r = 0.15, p_{vario}= 0.10	**r = 0.62,** p_{vario}< **0.001**
G2 (h^2)					r = 0.10, p_{vario}= 0.28	r = 0.24, p_{vario}= 0.008	r = 0.27, p_{vario}= 0.004	r = 0.13, p_{vario}= 0.02	**r = 0.24,** p_{vario}= **0.01**	r = 0.02, p_{vario}= 0.79
$G1_{SiC}$							**r = 0.52,** p_{vario}< **0.001**	**r = -0.56,** p_{vario}< **0.001**	r = 0.17, p_{vario}= 0.06	**r =0.80,** p_{vario}< **0.001**
$G2_{SiC}$							**r = -0.18,** p_{vario}= **0.05**	**r = 0.35,** p_{vario}< **0.001**	r = 0.23, p_{vario}= 0.02	r = -0.13, p_{vario}= 0.17
$G1_{GEN}$									r = -0.24, p_{vario}= 0.01	**r = 0.57,** p_{vario}< **0.001**
$G2_{GEN}$									r = 0.22, p_{vario}= 0.02	**r = -0.69,** p_{vario}< **0.001**
T1w/T2w										r = -0.26,p_{vario}= 0.01

Supplementary Table T3. Spatial similarity of dentate gyrus (DG) organisational axes computed in a pairwise fashion. Similarity is computed by Pearson's r and its significance reported by the p_{vario}; the p-value after spatial autocorrelation correction [77]. The autocorrelations were assessed by using the DG vertex coordinate and edge information as well as their n = 1000 simulated surrogate coordinates.

DG	$G1_{FC}$	$G2_{FC}$	G1 (h^2)	G2 (h^2)	$G1_{SiC}$	$G2_{SiC}$	$G1_{GEN}$	$G2_{GEN}$	T1w/T2w	Coupling
$G1_{FC}$			**r = 0.93,** p_{vario}< **0.001**	r =-0.04, p_{vario}= 0.69	**r = 0.88,** p_{vario}< **0.001**	r = 0.32, p_{vario}= 0.01	**r = 0.75,** p_{vario}< **0.001**	r = -0.19, p_{vario}= 0.14	r = 0.36, p_{vario}= 0.003	**r = 0.55,** p_{vario}< **0.001**
$G2_{FC}$			r = -0.31, p_{vario}= 0.01	**r = 0.74,** p_{vario}< **0.001**	r = -0.36, p_{vario}= 0.006	r = -0.15, p_{vario}= 0.02	r = -0.22, p_{vario}= 0.05	r = 0.23, p_{vario}= 0.05	r = -0.01, p_{vario}= 0.90	r = -0.34, p_{vario}= 0.01
G1 (h^2)					**r = 0.87,** p_{vario}< **0.001**	r = 0.27, p_{vario}= 0.03	**r = 0.65,** p_{vario}< **0.001**	r = -0.24, p_{vario}= 0.06	r = 0.37, p_{vario}= 0.004	**r = 0.54,** p_{vario}< **0.001**
G2 (h^2)					r = -0.18, p_{vario}= 0.14	r = -0.09, p_{vario}= 0.44	r = 0.04, p_{vario}= 0.75	r = 0.20, p_{vario}= 0.10	r = 0.05, p_{vario}= 0.71	r = -0.21, p_{vario}= 0.10
$G1_{SiC}$							**r = 0.70,** p_{vario}< **0.001**	**r = -0.57,** p_{vario}< **0.001**	**r = 0.43,** p_{vario}< **0.001**	**r = 0.70,** p_{vario}< **0.001**
$G2_{SiC}$							r = 0.19, p_{vario}= 0.12	**r = 0.65,** p_{vario}< **0.001**	**r = -0.45,** p_{vario}< **0.001**	r = -0.27, p_{vario}= 0.06
$G1_{GEN}$									r = 0.32, p_{vario}= 0.01	**r = 0.57,** p_{vario}< **0.001**
$G2_{GEN}$									**r = -0.43,** p_{vario}< **0.001**	**r = -0.55,** p_{vario}< **0.001**
T1w/T2w										r = 0.33,p_{vario}= 0.01

Supplementary Table T4.

Authors	Title	Dataset	Hippocampal Segmentations	Results
Whelan et al. 2016		QTIM* Cohort (n = 728) * *Queensland Twins Imaging*	Hippocampal fissure, Parasubiculum, Fimbria, HATA, CA3, Subiculum, CA4, Presubiculum, CA1, Granule cells of DG, Molecular Layer of DG, Hippocampal tail.	All regions exhibited high heritability in their volume: $0.56 \leq h^2 \leq 0.88$
Elman et al. 2019		VETSA*(n = 406) * *Vietnam Era Twin Study of Aging*	Hippocampal tail, Subiculum, CA1, Hippocampal fissure, Presubiculum, Parasubiculum, ML, GC-DG, CA3, CA4, Fimbria, HATA	All regions exhibited significant heritability in their volume (except for Hippocampal fissure): $0.57 \leq h^2 \leq 0.84$ Genetic correlations between total hippocampal volume and the subfields: $0.33 \leq r_g \leq 0.99$
Elman et al. 2019		HCP * (n = 556) * *Human Connectome Project*	Hippocampal tail, Subiculum, CA1, Hippocampal fissure, Presubiculum, Parasubiculum, ML, GC-DG, CA3, CA4, Fimbria, HATA	All regions exhibited significant heritability in their volume (except for Hippocampal fissure): $0.37 \leq h^2 \leq 0.89$ Genetic correlations between total hippocampal volume and the subfields: $0.55 \leq r_g \leq 0.98$
van der Meer et		16 different data cohorts*	Hippocampal tail, Subiculum, CA1,	All regions exhibited significant heritability in

al. 2020		(n = 21,297) * *PING, PNC, NIMAGE, UBA, BIG, UNIBA, TOP, HUBIN, DEMGEN, NCNG, UKBB, STROKEMRI, HUNT, BETULA, ADNI2, ADNI1*	Hippocampal fissure, Presubiculum, Parasubiculum, ML, GC-DG, CA3, CA4, Fimbria, HATA	their volume. $0.14 \leq h^2 \leq 0.27$ GWAS (genome wide association analysis) of whole hippocampal volume identified eight whole-genome significant loci.
Zhao et al. 2019	Heritability of Regional Brain Volumes in Large-Scale Neuroimaging and Genetic Studies *Cerebral Cortex*	UK Biobank (n = 9031 and number of SNPs* = 461,488) * *Single Nucleotide Polymorphism*	Whole-hippocampus	Significant SNP-heritability was addressed for the left hippocampal volume ($h^2 = 0.53$) and right hippocampal volume ($h^2 = 0.49$).
Warland et al. 2020	Schizophrenia-associated genomic copy number variants and subcortical brain volumes in the UK Biobank	UK Biobank (n = 441,333))	Whole-hippocampus	Hippocampal volume differences were significant for: > Schizophrenia (SZ)-associated CNV* carriers have reduced hippocampal volume compared to non-CNV carriers `> 15q11.2deletion* carriers have reduced hippocampal volume compared to non−CNV carriers (B = −0.46, SE = 0.18, p = 0.013, pFDR = 0.066)`

				** CNV: copy number variation* ** the most frequent SZ-CNV in the sample was 15q11.2deletion*

References

1. Yeo, B. T. T. *et al.* The organization of the human cerebral cortex estimated by intrinsic functional connectivity. *Journal of Neurophysiology* vol. 106 1125–1165 (2011).

2. Burt, J. B., Helmer, M., Shinn, M., Anticevic, A. & Murray, J. D. Generative modeling of brain maps with spatial autocorrelation. *Neuroimage* 220, 117038 (2020).